Single-cell profiling of tuberculosis lung granulomas reveals functional lymphocyte signatures of bacterial control

Authors:

Hannah P. Gideon[1, 2]*, Travis K. Hughes[3,4,5]*, Marc H. Wadsworth II[3,4,5,6], Ang Andy Tu[7], Todd M. Gierahn[7], Forrest F. Hopkins [4,8], Jun-Rong Wei [4,8], Conner Kummerlowe[9], Nicole L. Grant[1], Kievershen Nargan[10], JiaYao Phuah[1], H. Jacob Borish[1], Pauline Maiello[1], Alexander G. White[1], Sharie Keanne C. Ganchua[1], Amy Myers[1], Cassaundra L. Ameel[1], Catherine T. Cochran[1], Sarah K. Nyquist[3,4,5,9,12], Joshua M. Peters[4,7], Jaime A Tomko[1], Lonnie James Frye[1], Jacob M. Rosenberg[4,8,11], Angela Shih[11], Michael Chao[4,8], Charles A. Scanga[1,2], Jose Ordovas-Montanes[4,5], Bonnie Berger[12], Joshua T. Mattila[2,13], Rajhmun Madansein[14], J. Christopher Love[4,15,16], Bryan Bryson[4,7], Philana Ling Lin[2,17], Alasdair Leslie[10,18,19], Samuel M. Behar[20], JoAnne L Flynn[1,2#], Sarah M. Fortune[4,5,8#], Alex Shalek[3,4,5,6,16#]

***These first authors contributed equally to this work.**

#These last authors contributed equally to this work.

Authors Affiliation:

1. Department of Microbiology and Molecular Genetics, University of Pittsburgh School of Medicine, Pittsburgh PA USA
2. Center for Vaccine Research, University of Pittsburgh, Pittsburgh PA USA
3. Institute for Medical Engineering & Science, Massachusetts Institute of Technology, Cambridge, MA
4. Ragon Institute of MGH, MIT, and Harvard, Cambridge, MA
5. Broad Institute of MIT and Harvard, Cambridge, MA
6. Department of Chemistry, Massachusetts Institute of Technology, Cambridge, MA
7. Department of Biological Engineering, Massachusetts Institute of Technology, Cambridge, MA
8. Department of Immunology and Infectious Diseases, Harvard T.H. Chan School of Public Health, Boston, Massachusetts, USA
9. Program in Computational and Systems Biology, Massachusetts Institute of Technology, Cambridge, MA, USA.
10. Africa Health Research Institute, Durban, South Africa
11. Division of Infectious Diseases, Massachusetts General Hospital, Boston, MA

12. Computer Science and Artificial Intelligence Laboratory, Massachusetts Institute of Technology, Cambridge, MA, USA.
13. Department of Infectious Diseases and Microbiology, Graduate School of Public Health, University of Pittsburgh, Pittsburgh, PA
14. Deaprtment of Cardiothoracic Surgery, University of KwaZulu Natal, Durban, South Africa
15. Department of Chemical Engineering, Massachusetts Institute of Technology, Cambridge, Massachusetts, United States
16. The Koch Institute for Integrative Cancer Research, Massachusetts Institute of Technology, Cambridge, Massachusetts, United States
17. Department of Pediatrics, University of Pittsburgh School of Medicine, UPMC Children's Hospital of Pittsburgh, Pittsburgh PA USA
18. School of Laboratory Medicine and Medical Sciences, University of KwaZulu-Natal, Durban, South Africa.
19. Department of Infection and Immunity, University College London, London, United Kingdom
20. Department of Microbiology and Physiological Systems, University of Massachusetts Medical School, Worcester, Massachusetts, USA

Abstract

In humans and nonhuman primates, *Mycobacterium tuberculosis* lung infection yields a complex multicellular structure—the tuberculosis granuloma. All granulomas are not equivalent, however, even within the same host: in some, local immune activity promotes bacterial clearance, while in others, it allows persistence or outgrowth. Here, we used single-cell RNA-sequencing to define holistically cellular responses associated with control in cynomolgus macaques. Granulomas that facilitated bacterial killing contained significantly higher proportions of *CD4*+ and *CD8*+ T cells expressing hybrid Type1-Type17 immune responses or stem-like features and *CD8*-enriched T cells with specific cytotoxic functions; failure to control correlated with mast cell, plasma cell and fibroblast abundance. Co-registering these data with serial PET-CT imaging suggests that a degree of early immune control can be achieved through cytotoxic activity, but that more robust restriction only arises after the priming of specific adaptive immune responses, defining new targets for vaccination and treatment.

Introduction

Tuberculosis (TB), caused by *Mycobacterium tuberculosis* (Mtb), remains a major global health threat. It is estimated that one quarter of the world's population is infected with Mtb, and 10 million new cases and 1.5 million deaths due to TB were reported in 2019 (WHO, 2019). More than 90% of those infected do not progress to active disease. Thus, protective immune responses against Mtb appear to be relatively common in humans, but have been difficult to dissect because of our inability to measure immune responses in lung tissue and to distinguish the true extent of bacterial control in people. Understanding the cellular and molecular features associated with protective immunity, as well as those that lead to failure to control infection, is critical for the development of next-generation cures and preventions for TB.

Mtb infection in humans and nonhuman primates (NHP) is characterized by the formation of granulomas predominantly in the lungs and lymph nodes (Flynn, 2010; Lin et al., 2014b; Russell et al., 2010; Ulrichs and Kaufmann, 2006). TB lung granulomas are spatially organized structures (**Figure 1A**), well circumscribed from the lung parenchyma and comprised of a combination of parenchymal, stromal, and immune cells, such as macrophages, neutrophils, T cells, B cells and plasma cells (Ehlers and Schaible, 2012; Flynn, 2010; Gideon et al., 2019; Lin et al., 2006; Mattila et al., 2013; Pagan and Ramakrishnan, 2014; Phuah et al., 2012; Reece and Kaufmann, 2012; Ulrichs and Kaufmann, 2006). A spectrum of granuloma types, organization and cellular composition have been described in both humans and NHP (Canetti, 1955; Flynn, 2010; Hunter, 2011, 2016; Lin et al., 2006).

The cynomolgus macaque NHP model of Mtb infection has been critical for characterizing the cellular and molecular features that underlie granuloma fate since it recapitulates the spectrum of human infection outcomes, disease and pathology (Canetti, 1955; Flynn, 2010; Lin et al., 2006) and. Human granulomas are typically available only from surgical resections in cases

where drug treatment fails and thus do not allow analysis of successful immune clearance. Most murine models, meanwhile, do not develop human-like granulomas, and mice are not particularly adept at killing Mtb bacilli in the lungs, which makes identifying features associated with immune mediated clearance difficult (Flynn et al., 2015; Flynn, 2010; Langermans et al., 2001; Verreck et al., 2009; Zhan et al., 2017).

Studies of Mtb infection in NHP have demonstrated that individual granulomas are dynamic (Coleman et al., 2014b; Lin et al., 2013; Lin et al., 2014b), changing with the evolving interactions between bacteria and diverse host cell types (Ehlers and Schaible, 2012; Flynn et al., 2003; Flynn, 2010; Mattila et al., 2013; Phuah et al., 2012; Ulrichs and Kaufmann, 2006). The bacterial burden in individual granulomas is highest early in infection and then decreases due to increased killing as the immune response evolves, even in animals that ultimately develop active TB **(Figure S1A-B**) (Cadena et al., 2016; Lin et al., 2014b; Maiello et al., 2018). Strikingly, however, individual granulomas within a single host follow independent trajectories with respect to inflammation, cellular composition, reactivation risk, and ability to kill Mtb (Coleman et al., 2014b; Gideon et al., 2015; Lenaerts et al., 2015; Lin et al., 2013; Lin et al., 2014b; Malherbe et al., 2016; Martin et al., 2017). We and others have systematically profiled cellular immune responses of individual cell types in macaque lung granulomas, including T cells (Diedrich et al., 2020; Foreman et al., 2016; Gideon et al., 2015; Lin et al., 2012; Mattila et al., 2011; Wong et al., 2018), macrophages (Mattila et al., 2013), B cells (Phuah et al., 2016; Phuah et al., 2012), and neutrophils (Gideon et al., 2019; Mattila et al., 2015), and examined the instructive roles of cytokines including IFN-γ, IL-2, TNF, IL-17 and IL-10 (Gideon et al., 2015; Lin et al., 2010; Wong et al., 2020). These analyses have enabled key insights into how specific canonical cell types and effector molecules relate to bacterial burden; for example, they revealed that balanced production of pro- and anti-inflammatory cytokines by granuloma T cells associates with bacterial control. However, each analysis has been relatively narrow in focus

and we have little understanding of how the collective actions of diverse cell types within individual granulomas shape outcome.

The recent emergence of high-throughput single-cell genomic profiling methods affords transformative opportunities to define the cell types, phenotypic states and intercellular circuits that comprise granulomas and inform their dynamics (Prakadan et al., 2017). Rather than forcing selection of distinct cellular subsets or features of interest *a priori*, single-cell RNA-Seq (scRNA-seq) can be applied to examine comprehensively the cellular constituents of complex multicellular structures and their functional attributes. Illustratively, single-cell transcriptomics has been used to identify fundamental alterations in cellular ecosystems associated with the severity and persistence of inflammation (Ordovas-Montanes et al., 2018; Smillie et al., 2019), the cellular bases of disease (Kazer et al., 2020; Montoro et al., 2018) and responses to it, and actionable features of the tumor-immune microenvironment (Hovestadt et al., 2019; Tirosh et al., 2016). While scRNA-seq has been applied to understand peripheral immune or *in vitro* responses in Mtb infection (Gierahn et al., 2017; Huang et al., 2019; Nathan et al., 2020), it has yet to be leveraged to empower global analyses of cellular responses linked to bacterial control in TB lung granulomas, potentially given challenges associated with tracking, identifying, and isolating these small heterogeneous structures from NHP in a biosafety-level 3 suite.

Here, to characterize the relationship between the cellular features of TB lung granulomas and bacterial burden explicitly, we applied the Seq-Well platform for massively-parallel single-cell RNA-Seq (scRNA-seq) (Gierahn et al., 2017) to generate single-cell transcriptional profiles of pulmonary Mtb granulomas at 10 weeks post infection (p.i.; **Figure 1A**) in cynomolgus macaques. Individual granulomas displayed a broad range of bacterial burdens from restrictive (sterile, 0 colony forming units (CFU) – i.e., culturable live bacterial burden) to permissive (high, ~80,000 CFU), enabling us to define cellular compositions and effector functions that associate

with bacterial control. With these data, based on unbiased gene-expression analysis, we discovered several previously unappreciated functional cellular phenotypes that are temporally associated with bacterial control – including hybrid T1-T17 CD4+ and CD8+ states, cytotoxic T and NK subsets, mast, and plasma cells – and validate select observations and extend to humans via orthogonal techniques. Collectively, our data provide a global view of the TB lung granuloma cellular microenvironments in which Mtb is either controlled or persists, suggesting several novel therapeutic and prophylactic targets for future investigation.

Results

Study design and bacterial burden in granulomas

We sought to comprehensively define the complex cellular ecosystems (**Figure 1A**) of granulomas that manifested different degrees of bacterial control in NHP. Four cynomolgus macaques were bronchoscopically infected with a low dose of Mtb (<10 CFU; Erdman strain) and followed for 10 weeks (**Figure 1B**). The 10-week timepoint represents the first time at which a significant reduction in average granuloma-level bacterial burden is observed, compared to peak burden at 4 or 6 weeks post infection (p.i.) (**Figure S1A-B**). Progression of Mtb infection and granuloma formation were monitored using PET-CT scans at 4, 8, and 10 weeks p.i. For each animal, we quantified total lung FDG activity (**Figure 1C**) from PET-CT scans as a proxy for overall inflammation (Coleman et al., 2014b; White et al., 2017). At necropsy, individual PET-CT identified lung granulomas were excised and dissociated to obtain a single-cell suspension (**STAR* Methods**).

Twenty-six granulomas from the four animals were randomly selected for profiling by scRNA-seq. For each, we further quantified viable bacterial burden (CFU – i.e., culturable live bacterial burden) and cumulative (live + dead) bacterial load (chromosomal equivalents, CEQ) (Lin et al., 2014b; Munoz-Elias et al., 2005) (**Table S1, STAR* Methods**). Among the 26 granulomas, there was a range of granuloma-level bacterial burdens, from sterile (0 CFU/granuloma) to high burden (4.6 $\log_{10}$ CFU/granuloma) lesions (**Figure 1D**). We analyzed the granulomas using CFU both as a continuous variable and by binning it into tertiles (Low: 0-500 CFU, n=10; Mid: 500-5000 CFU, n=10; and High: >5000 CFU, n=6) which displayed significant differences in bacterial burden (low-CFU: median 1.9 $\log_{10}$ CFU/granuloma, mid-CFU 3.4 $\log_{10}$ CFU/granuloma, high-CFU: 4.2 $\log_{10}$ CFU/granuloma; $p<0.0001$, Kruskal-Wallis test with Dunn's multiple testing correction) (**Figure 1E** and **Table S1)**.

We evaluated cumulative bacterial burden (chromosomal equivalents, CEQ – derived from live + dead Mtb) to determine whether low CFU reflected reduced bacterial growth or increased bacterial killing (Cadena et al., 2018; Lin et al., 2014b; Munoz-Elias et al., 2005). We observed no significant difference in CEQ values between granulomas with low and high CFU ($p>0.99$, Kruskal-Wallis test with Dunn's multiple testing correction) (**Figure 1F**), indicating that granulomas supported roughly similar cumulative Mtb growth over the course of infection. To quantify the extent of bacterial killing, we calculated the ratio of CFU to CEQ (**Figure 1G**; **STAR* Methods**). Granulomas with the lowest bacterial burdens had significantly higher killing (-2.1 $\log_{10}$ CFU/CEQ per granuloma) than those with the highest bacterial burden (-0.63 $\log_{10}$ CFU/CEQ per granuloma, $p=0.0051$, Kruskal-Wallis test with Dunn's multiple testing correction; **Figure 1G**).

Cellular composition of TB lung Granulomas

To identify cellular and molecular factors associated with increased Mtb killing in an unbiased fashion, we applied a single-cell suspension from each granuloma to a Seq-Well array preloaded with barcoded mRNA capture beads under Biosafety Level 3 conditions, and processed and sequenced as previously described (**STAR* Methods**) (Gierahn et al., 2017). After aligning the data to the *Macaca fascicularis* (cynomolgus macaque) genome and performing robust quality controls and granuloma-specific technical corrections, we retained 109,584 high-quality single-cell transcriptomes for downstream analysis (**Figure S2; Table S2; STAR* Methods**).

Unsupervised investigation of these data revealed 24 distinct clusters, which we assigned to canonical cell types using a combination of manual curation and reference gene expression signatures from the Tabula Muris (Tabula Muris et al., 2018), Mouse Cell Atlas (Han et al., 2018) and SaVanT database (Lopez et al., 2017) (**Figure S3 A-H; STAR* Methods**). Based on

shared expression of genes associated with canonical cell types, we reduced these 24 clusters to 13 general cell type clusters (**Figures 2A** and **S3G-H**). These encompass groups of lymphocytes, including B cells (defined by expression of *MS4A1*, *CD79B*, & *BANK1*), T and NK cells (T/NK; *GNLY, TRAC, CD3D,* & *GZMH*) and plasma cells (*IGHG1* & *JCHAIN)*); myeloid cells, including conventional dendritic cells (cDCs; *CLEC9A, CST3,* & *CPVL*), plasmacytoid dendritic cells (pDCs; *LILRA4* and *IRF8*) and macrophages (*APOC1, LYZ,* and *APOE*); mast cells (*CPA3* & *TPSAB1*); neutrophils (*CCL2, CXCL8,* & *CSF3R*); erythroid cells (*HBA1* & *HBB*); stromal cells, including endothelial cells (*RNASE1, EPAS1,* & *FCN3*) and fibroblasts (*COL3A1, COL1A1,* & *DCN)*; Type-1 pneumocytes (*AGER*); and, Type-2 pneumocytes (*SFTPC, SFTPB,* and *SFTPA1*) (**Figure 2A & B, Figure S3G-H** and **Table S3**).

Granuloma cellular composition is associated with bacterial burden

To investigate the relationship between cell type composition and bacterial burden, we quantified the correlation between cellular frequency and CFU across all granulomas (**Figure 2C, Figure S3I, Table S8**). We also assessed differences in cell type proportions between granulomas with low and high bacterial burden **(Figure 2D, Table S8)**, and relied on this analytic approach for some sub-state analyses where our granuloma numbers were too small to perform a robust correlation analysis. The associations identified when the extent of bacterial killing was treated as a discrete variable were highly consistent with those identified when it was treated as a continuous variable (**STAR* Methods**).

There was a negative correlation between bacterial burden and the proportion of cells from the unified T and NK cell cluster, and surprising positive correlations between bacterial burden and plasma cells, endothelial cells, mast cells, fibroblasts and type-1 pneumocytes (**Figure 2C-D**, **Table S8A**). We did not observe a significant association between macrophage abundance and

bacterial burden. This was true when we examined all 27,670 macrophages as a single cluster, or when we assessed each of the 9 macrophage sub-clusters identified through further analysis to resolve their substantial heterogeneity, as reported in other studies (Zilionis et al., 2019) (**Figure S4** and **Table S4; STAR* Methods**).

T and NK cells as mediators of protection

Our initial analysis revealed a unified T and NK cell cluster that was, in aggregate, the only cell population negatively correlated with bacterial burden (**Figure 2C-D**). Data from human and animal models (including NHPs) suggest an important role for diverse lymphocyte populations in controlling Mtb infection. In addition to compelling evidence for the importance of conventional CD4+ and CD8+ T cells (Chen et al., 2009; Foreman et al., 2016; Lin and Flynn, 2015; Lin et al., 2012; Mogues et al., 2001), other lymphocyte populations have been implicated in control including gamma delta (γδ) T cells (Ogongo et al., 2020; Shen et al., 2019), iNKT cells (Arora et al., 2013; Chackerian et al., 2002; Chancellor et al., 2017), donor-unrestricted T cells such as MAITs (Joosten et al., 2019), innate lymphoid cells (ILC) (Ardain et al., 2019) and cytotoxic lymphocytes including NK cells (Lin and Flynn, 2015; Portevin et al., 2012; Roy Chowdhury et al., 2018).

To further assess functional diversity within the 41,622 cells that comprise T and NK cell cluster, we performed additional analysis and identified 13 subclusters (designated numerically in **Figure 3A and S5 Table S6**; **STAR* Methods**). We annotated each subcluster of the unifed T and NK cluster based upon enrichment of distinct transcriptional features **(Figure 3C)**, focusing on those that associate with bacterial control. The abundance of 6 subclusters was negatively correlated with bacterial burden **(Figure 3D,Table S8b)**; of these, 4 are relatively abundant clusters comprising 2.4-8.7% of all granuloma cells while 2 constitute less than 1% of all

granuloma cells **(Table S4c)**. There were no T and NK subclusters that positively correlated with bacterial burden.

To further describe each subcluster and identify features that associate with bacterial control, we first examined the expression of lineage defining markers, known cytotoxic, regulatory, proliferation genes and T cell transcription factors (**Figure 3C** and **Figure S5D-F)** and assessed TCR constant gene (*TRAC*, *TRBC* and *TRDC*) expression (**Figure 3B).** The process of annotation revealed that most of the agnostically defined subclusters did not correspond neatly to canonical T and NK cell populations. Where possible, we annotate subclusters based on known T cell markers and literature derived genes of interest but these are parts of broader transcriptional signatures that appear to reflect dominant cellular response states superimposed on cell lineage-associated gene expression programs.

A prominent role for Type1-Type 17 T cells in bacterial control

T and NK subcluster 13 was the most abundant cell type across all granulomas (8.8%) and the strongest correlate of control (**Figure 3A,D**; **Table S4c & S8b**). In this subcluster, we observe enriched expression of classical Th1-associated genes including *IFNG* and *TNF* (Raphael et al., 2015), as well as elevated expression of transcription factors associated with Th17 differentiation (Yosef et al., 2013) including *RORA* (Yang et al., 2008), *RORC* (Ivanov et al., 2006), *RBPJ* (Meyer Zu Horste et al., 2016) and *BHLHE40* (Huynh et al., 2018; Lin et al., 2016; Lin et al., 2014a). Although this subcluster is also enriched for additional features of Th17 cells including *CCR6* (Hirota et al., 2007) and *IL23R (Kobayashi et al., 2008)*, we do not observe expression of *IL17A* or *IL17F* (**Figure 4A; Table S6)**.

This hybrid gene expression state is consistent with previously described expression programs for Th1* or ex-Th17 cells. Th1* cells are a subset of Th1 cells, characterized by expression of

CCR6 and *CXCR3*, that co-express IFN-γ and T-bet in addition to RORγt, and are postulated to play a role in antigen-specific memory (Acosta-Rodriguez et al., 2007), and in human blood, memory CD4 T cells with a Th1* expression profile were enriched in individuals with latent TB compared to uninfected controls (Burel et al., 2018). Ex-Th17 cells, meanwhile, represent precursors to long-lived tissue-resident memory, characterized by increased expression of *RBPJ*, *BHLHE40*, *IL23R* and *IL7R* and minimal ROR-γT and IL-17 (Amezcua Vesely et al., 2019). Previous studies have revealed a prominent role for CD4 Th1 and Th17 cytokines in control of Mtb infection, including IFN-γ, TNF, and IL-17 (Algood et al., 2005; Green et al., 2013; Khader et al., 2007; Khader and Gopal, 2010; Lin et al., 2007; Lyadova and Panteleev, 2015; Millington et al., 2007; O'Garra et al., 2013; Scriba et al., 2017), and studies in NHP granulomas suggest an association between T1 and T17 cytokine expression and bacterial burden (Gideon et al., 2015). In addition, in murine models, BHLHE40 is required for control of Mtb infection, as a repressor of IL-10 production (Huynh et al., 2018).

While Th1* and exTH17 subsets have been described primarily as CD4 T cells, this T1-T17 subcluster is characterized by the expression of both *CD4* and *CD8A/B* transcripts **(Figure 3C, Figure S5D-E)**. Moreover, when we compared the gene expression patterns of CD4 and CD8 expressing cells in the subcluster, we noted differential expression of biologically relevant genes. We therefore questioned whether this subcluster might consist of subpopulations of cells representing canonical cell types. Upon further subclustering of 9,234 T1-T17 cells, we identified 4 distinct subpopulations **(Figure 4B, Table S7**). Critically, each expresses genes associated with a Th1* or ex-Th17 state including IL23R, CCR6, and CXCR3, as well as *RBPJ*, *BHLHE40, FURIN, RORA* and *COTL1*. However, each subpopulation also expresses unique transcriptional programming. Specifically, T1-T17 subpopulation 1 is characterized by expression of *CD4* and markers of activation and motility including *IL7R*, *CD6*, *TXNIP*, *PDE4D*,

ZFP36L2, *ITGB1*, *CCR6 and CXCR3* (**Figure 4C-D**), and has distinct transcriptional overlap with T and NK subcluster 7 (stem-like cells, decribed below). Although we cannot confidently assign effector functions to this subpopulation from the transcriptional data, they are reminiscent of memory cells with restrained metabolic activity and cytokine expression. T1-T17 subpopulation 2 is characterized by increased relative expression of cytotoxic effector molecules including *GZMA*, *GZMH*, *GZMK*, *GNLY*, *PRF1*, *KLRC1* and both *CD8A* and *CD8B* (**Figure 4C-D**). T1-T17 subpopulation 3, which includes cells expressing *CD8A/B* or *CD4*, is characterized by cytokine gene expression (*IFNG, TNF, LTA*, and *LTB),* markers of an inhibitory cell state (*CTLA4*, *GADD45B* and *SLA*) and expression of genes implicated in glycolysis and mTOR signaling (*TPI1, PKM HSPA5, ENO1*) **(Figure 4C-D)**. T1-T17 subpopulation 4 is very low in abundance and characterized by heat shock and DNA damage associated transcripts (*DNAJB1* and *HSPH1*) (**Figure 4**, **Table S4D)**.

Low-burden granulomas had increased abundance of T1-T17 subpopulation 1 (p=0.0324, Kruskal Wallis with Dunn's multiple testing corrections), subpopulation 2 (p=0.0302) and subpopulation 4 (p=0.0152) compared to high-burden granulomas, suggesting a prominent role for both helper and cytotoxic functions of T1-T17 T cells (**Figure 4E**, **Table S8C**). However, there was a significant negative correlation only between T1-T17 subpopulations 2 and CFU (Spearman's rho -0.4482, P=0.0216), revealing an unexpected association of cytotoxic effectors in the control of Mtb. Surprisingly, T1-T17 subpopulation subpopulation 3 was not correlated with bacterial burden, despite expressing elevated levels of *IFNG* and *TNF* (**Figure 4E**, **Table S8C**), genes generally considered as critical to control Mtb infection (O'Garra et al., 2013; Scriba et al., 2017).

Additional cytotoxic features associated with bacterial control

Additional T/NK cell subcluster correlates of control reinforce an association between cytotoxicity and bacterial burden **(Figure 3D, Table S8C)**. Subcluster 4, constituting 3.8% of granuloma cells, is one of the six primary subclusters (1-6) defined broadly by cytotoxic features, such as expression of genes for granzymes (*GZMA, GZMB, GZMH, GZMK* and *GZMM*), granulysin (*GNLY)*, or perforin (*PRF1*) **(Figure 3C)**. Three of these subclusters (subclusters 1, 3, 4) are enriched for polyfunctional cytotoxic cells, characterized by the expression of multiple cytotoxic effector genes, while subclusters 2, 5 and 6 are distinguished by a more limited number of cytotoxic features.

Subcluster 4 is enriched for expression of *PRF1, GZMH*, *GZMB,* and *GZMM*, but not *GNLY*, a pattern consistent with that described for dicytotoxic CTLs (Balin et al., 2018) In addition, it is enriched for genes implicated in motility, migration and tissue residency, including *CX3CR1, TGFBR3*, and *S100A10*, and regulators of cell state such as *AHNAK*, *KLF3*, and *ZEB2* (**Figure 3D-E; Table S7**). Further, subcluster 4 is enriched for expression of both *CD8A* and *CD8B*, and expresses *TCRA* and *TCRB* but not *TCRD* **(Figure 3B-C, Figure S5E-F)**, suggesting that it is largely composed of conventional CD8αβ T cells (Fan and Rudensky, 2016). There are a small number of *CD4*-expressing cells in this subcluster which do not differ from the *CD8A* and *CD8B*-expressing cells in their expression of the subcluster defining genes **(Figure S5E-F)**. Subcluster 4 is also enriched for expression of markers that can be expressed either by cytotoxic CD8 cells or NK cells, including *KLRD1, KLRF1, KLRK1* and *NKG7* **(Figure 3C)**.

We sought to identify features that distinguished subcluster 4 from other subclusters that share cytotoxic features but are not associated with control. In contrast to subcluster 4, subcluster 1 (4.3% granuloma cells, **Table S4C**), is characterized by high expression of all three classes of cytotoxic effectors genes—*GNLY*, *PRF1 and GZMH*, *GZMA GZMB*—as well as *KLRD1, KLRC1*, *KLRC2*, *NKG7*, and shares some features with previously described tricytoxic CD8+

cells (Balin et al., 2018). Subcluster 1 is enriched for the expression of *CD8A* but not *CD8B*, and has the highest proportion of TCRD expressing cells **(Figure 3B-C, Figure S5E-F, Table S8B)**. Taken together, the data suggest that subcluster 1 contains a greater proportion of highly cytotoxic innate CD8+ T cells (possibly NKT cells), γδ T cells, and natural killer cells (NK) than subcluster 4. Subcluster 3, (0.4% of granuloma cells, **Table S4C**), which also does not correlate with control, appears to be more selectively enriched for NK cells as it is defined both by enrichment for cytotoxic and NK cell markers but also relatively low expression of *CD3D* and *CD3G* **(Figure 3C, Table S8BB)**. Subcluster 5, representing 4.7% of granuloma cells, displayes elevated expression of only a single cytotoxic marker, *GZMK*, which does not activate apoptotic caspases (Guo et al., 2010). Cytotoxic subcluster 6, meanwhile, is a very low abundance cluster (<0.3%) about which we cannot draw meaningful conclusions.

The most revealing comparision was between subclusters 4 and 2 (1.9% of granuloma cells). Subcluster 2 is also enriched for NK and CD8 cell lineage marker expression such as *KLRC1, KLRB1, KLRG1, CD8A* and *TCRD* but is only moderately enriched for *PRF1* expression, and is not characterized by the expression of any other cytotoxic effector or cytokine genes **(Figure 3B-C)**. Interestingly, subcluster 2 is highly enriched for expression of activation markers *CD69* and *NR4A1* (Nur77) and for expression of *EGR1, EGR2* and *DUSP2,* a trio of transcription factors described to distinguish peripherally tolerant CD8 T cells in a model of tumor infiltrating lymphocytes (Schietinger et al., 2012). Strikingly, subcluster 2 is additionally defined by the expression of genes implicated in the inhibition of NFkB signaling, *NFKBIA* (IkB), *NFKBIZ* and *TNFAIP3*, but not markers suggestive of T cell exhaustion **(Figure 3C)**. Taken together, these data suggest that cells in subcluster 2 are undergoing TCR activation but not undertaking effector functions and may be in an expression state suggestive of peripheral tolerance. The functional complexity of these subclusters, and the common and distinct responses they represent, supports a significant and underappreciated role for cytotoxic cells in TB granulomas

and suggests a need to further elucidate actionable avenues for plasticity for future preventions and cures.

Stem-like T cell function in TB lung granulomas

Subcluster 7 (8.3% of granuloma cells, **Table S4C**) also correlates with control and is characterized by elevated expression of markers of naïve or memory CD4 and CD8 T cells including *TCF7*, *CCR7, IL7R,* and *TXNIP,* as well as genes associated with activation or memory state such as *CD69* and *ITGB1* (**Figure 3C-D**). These cells may represent a "stem-like" population of T cells, which are described as an early differentiating memory phenotype, distinct from naïve T cells, that are long-lived and possess a unique ability to proliferate and self-renew (Ahmed et al., 2016; Caccamo et al., 2018; Gattinoni et al., 2011). Similar cells have been reported in human and animal models of viral infection (Cartwright et al., 2016; Fuertes Marraco et al., 2015) and tumors (Ando et al., 2020; Brummelman et al., 2018; Wu et al., 2019), and in humans with Chagas disease (Mateus et al., 2015). In the tumor microenvironment, stem-like T cells have been described as expressing inhibitory receptors such as PD-1 (Siddiqui et al., 2019). This population is thought to undergo a proliferative burst after immune checkpoint blockade. By contrast, we do not identify enhanced expression of transcripts encoding inhibitory receptors in the stem-like subcluster **(Figure 3C)**. Indeed, inhibitory receptor transcripts are only expressed highly on cells in subcluster 8 (1.2 % of granuloma cells), which appear to be regulatory T cells (Tregs) based on elevated expression of canonical Treg markers (*FOXP3, CTLA4, CGA, TIGIT, TNFRSF18, IL1RL1,* and *IKZF4*) **(Figure 3C)**. The abundance of subcluster 8 neither positively nor negatively correlates with bacterial burden **(Figure 3D, Table S8B)**.

Additional T/NK cell subclusters that correlate with control

There were 3 additional T/NK subclusters that correlated with bacterial burden **(Figure 3D, Table S8B)**. Subcluster 10 was a small *CD4* enriched subcluster (0.05%) defined by metallothionein genes such as *MT1* and *MT2* **(Figure 3C-D)**; metallothionein-expressing T cells may play a role in negative regulation of Type 1 regulatory (Tr1) CD4+ cells (Wu et al., 2013). Subcluster 11 was relatively abundant (2.4% of granuloma cells, **Table S4C**) and was characterized by expression of transcripts associated with cellular proliferation (*MKI67*, *STMN1*, and *TOP2A*) **(Figure 3C-D, Table S8B)**, consistent with published data that T cell proliferation occurs within NHP and human granulomas (Gideon et al., 2015; McCaffrey et al., 2020; Ohtani, 2013; Phuah et al., 2016; Phuah et al., 2012; Wong et al., 2018). Subcluster 12, representing 0.6% of granuloma cells, is characterized by enrichment of genes associated with nuclear speckles and splicing factors such as *PNISR* and *SRRM2* **(Figure 3C)**, the latter of which has been associated with alternate splicing in Parkinson disease (Shehadeh et al., 2010) and has a critical role in organization of 3D genome (Hu et al., 2019).

T/NK cell subclusters that do not correlate with granuloma infection outcome

There are 2 relatively abundant subclusters of lymphocytes that have gene expression profiles consistent with known cell types but which do not correlate with control, either positively or negatively **(Table S8B)**. As noted above, one is subcluster 8, which displays elevated expression of canonical Treg markers (*FOXP3, CTLA4, CGA, TIGIT, TNFRSF18, IL1RL1,* and *IKZF4*) (Niedzielska et al., 2018; Zemmour et al., 2018) (**Figure 3C**) and *GATA3*, a Th2 lineage-defining transcription factor that has been observed in a subset of tissue-resident Tregs (Whibley et al., 2019). The second is subcluster 9, which is enriched for CD4 expression and Type-I interferon inducible molecules (*MX1*, *ISG15*, *IFIT3*, *IFI6*, *IFIT1*, *RSAD2*, and *MX2*) (Szabo et al., 2019) and may represent activated CD4+ T cells **(Figure 3C)**. Despite expectations that activated CD4+ T cells are critical mediators of TB control, the abundance of this population does not correlate with control at this time point.

Relationship between timing of granuloma formation and granuloma composition

In this study, the time of granuloma appearance was tracked through serial PET-CT scans (Coleman et al., 2014b; Lin et al., 2013; Martin et al., 2017). In further examining the serial PET-CT scans for the four animals in the current study, we found that 15 of the granulomas randomly chosen for scRNA-seq were observed at 4 weeks p.i. (i.e., "early-detected" granulomas following Mtb infection), while another 11 were only seen at 10 weeks p.i. (i.e., "late-detected" granulomas) (**Table S1**). Late-detected granulomas may be formed through dissemination (Martin et al., 2017); alternatively, some granulomas may take more time to reach the inflammatory threshold required to be identified by PET-CT scans (limit of detection $\geq$1mm), potentially because of slower bacterial growth or more efficient immune control.

There was a striking difference (~40-fold) in granuloma-level bacterial burden (CFU) between early- (n=15, 3.6 $\log_{10}$ CFU/granuloma, IQR: 3.2-4.6) and late-detected granulomas (n=11, 2 $\log_{10}$ CFU/granuloma, (0-2.8)) ($p<0.0001$) (**Figure 5A**) **Table S10a**), although median size and granuloma FDG avidity were similar among all 26 at 10 weeks p.i. (**Table S1)**. Critically, while there is a trend towards lower cumulative bacterial burden in late-detected lesions, the granuloma-level CEQ values were not significantly different between early- and late-detected granulomas ($p=0.0737$) (**Figure 5B, Table S10A**), suggesting that the lower bacterial burden (CFU) in new lesions was not strictly attributable to reduced bacterial growth. Moreover, the CFU/CEQ ratio (which is an inverse measure of bacterial killing) (Lin et al., 2014b) was ~10 fold lower in late-appearing granulomas ($p=0.0107$), indicating increased bacterial killing in those lesions. Comparison of cell-type proportions revealed that early- and late-detected granulomas were also characterized by differences in cellular composition. Many of the associations between cellular frequency and bacterial control were reflected in the differences between early and late lesions, including those with mast cells, plasma cells and the unified T/NK cell cluster,

as well as those with T/NK subclusters 13 (T1-T17) cells, 4 (cytotoxic) and 7 (stem-like T cells) (**Figure 5D-E**).

Bacterial control in early detected granulomas is associated with cytotoxic function

We sought to gain further insight into bacterial control specifically in the early appearing granulomas, which likely represent the original establishment of infection. We contrasted the early granulomas with the highest CFU (n=6, median CFU: 17,550, 4.2$\log_{10}$) and lowest CFU (n=6, median CFU: 2355, 3.3$\log_{10}$) (p=0.002, Mann-Whitney U) (**Figure 5F, Table S10)**. In early-detected lesions with lower burden, there was again a significantly higher proportion of T/NK subclusters 4 (p=0.009, Mann-Whitney U) and 5 (p=0.004), 7 (stem-like T cells) (p=0.041), 10 (p=0.004) and subcluster 13 (T1-T17 cells) (p=0.041) (Figure 5H). However, this analysis also revealed previously unappreciated associations between lower bacterial burden in early granulomas and additional subclusters of T/NK cells. These include the cytotoxic subclusters 1 (p=0.041) and 2 (p=0.002) (**Figure 5H, Table S10**) and the T1-T17 subpopulation 3 marked by *IFNG* and *TNF* (p=0.026) **(Table S5c, Table S10)**. Taken together, these data suggest a prominent role for cytotoxic function and otherwise cryptic role for Type 1 cytokines, possibly from innate or early adaptive lymphocytes, in the initial control of Mtb infection.

TCR repertoires of TB lung granulomas

Given the strong association between the abundance of specific T cell phenotypes and control of Mtb, we wondered whether these T cells might target common antigens (i.e., share common T cell receptors; TCRs). To investigate whether there was clonal enrichment among T cells, we reconstructed CDR3 sequences from granuloma T cells by performing targeted pulldowns of $\alpha\beta$ TCR sequences from the granuloma whole transcriptome amplification libraries to generate secondary sequencing libraries (**STAR* Methods**) (Tu et al., 2019). Initially, we examined the extent of TCR-α and TCR-β recovery and enrichment (i.e. CDR3-α, n $\geq$10; CDR3-β sequences,

n ≥12; CDR-αβ, n ≥10) across the T and NK subclusters and observed enrichment of common CDR3 sequences in the T1-T17 and proliferating subclusters (13 and 11, respectively), as well as cytotoxic subclusters 4 and 5 (**Figure S6A-D, Table S9; STAR* Methods**). Next, we examined sharing of enriched CDR3 sequences between granulomas. While we failed to observe public TCRs between animals (**Figure S6E)**, within an animal (e.g., monkey 4017), there was substantial sharing of TCR-α and TCR-β CDR3 sequences across lesions, including extensive sharing of CDR3 sequences between high-burden and low-burden granulomas (**Figure S6E**). This suggests that TCR enrichment is not strictly dependent on bacterial burden, and that antigens seen by enriched T cell clones may be similar in restrictive and permissive granulomas.

We further investigated the relationship between CDR3 sequence, T cell phenotypes and granuloma-level CFU. We observed associations between CDR3 sequence and T/NK cell sub-cluster populations within enriched CDR3 sequences (**Figure S6F**). For example, we identified individual CDR3s where the majority of cells are derived from either the subcluster 13 (T1-T17) or 4 or 5 (cytotoxic). In cases where a single affinity receptor is associated with multiple subclusters, the two transcriptional phenotypes observed are typically T1-T17 and proliferating T cells (**Figure S6F**). In the animal with the broadest distribution of bacterial burdens among the randomly selected granulomas (monkey 4017), the enriched CDR3 sequences shared similar cellular phenotypes across high and low burden lesions (**Figure S6G, Table S14**). Taken together, these data do not support the hypothesis that T cell specificity defines bacterial control at the level of the granuloma.

Finally, we leveraged targeted TCR reconstruction data to identify rare populations of donor-unrestricted T cells (DURTs; **STAR* Methods**), which represent a heterogenous class of

invariant T cells, including mucosal associated invariant T (MAIT) cells, invariant natural killer T cells (iNKT cells), and CD1 restricted Germline-Encoded Mycolyl lipid reactive (GEM) T cells (Ogongo et al., 2020; Van Rhijn et al., 2015). Among DURTs, we observe the highest frequency of T cells with the TRAV1-2/TRAJ33 MAIT-associated TCR combination (240/9,281 (number of T cells with alpha recovery), 0.6% of total T cells), a population of iNKT cells (TRAV10-1/TRAJ18) TCR sequences (20/9,281, 0.05%) and GEM cells (TRAV1-2/TRAJ9) (5/9,281) (**Figure S6H**). Rather than defining a distinct phenotypic subset, we found that these cells distributed across several T and NK cell subclusters. Their low frequency precluded an accurate assessment of their relationship to granuloma-level bacterial burden.

Cellular ecology of pulmonary TB granulomas

To assess whether specific cell types co-reside in TB lung granulomas more than would be expected by chance, we calculated the pairwise Pearson correlation matrix between all major cell types and sub-clusters across 26 granulomas (**Figure 6A; STAR* Methods**). Using hierarchical clustering of this pairwise correlation matrix, we defined 5 primary groups of cell clusters/sub-clusters whose abundances are associated across granulomas (**Figure 6A, Table S11**). Of these, group 2 (“Red”), which includes mast cells, plasma cells and certain stromal populations, is significantly expanded in high-burden and early-detected lesions compared to low burden, late lesions. Group 4 (“Teal”), which primarily consists of T cell subclusters, is significantly higher in low burden and late-detected granulomas compared to high burden and early-detected granulomas (**Figure 6B, Table S12**).

Given the unexpected increased frequency and co-occurrence of plasma and mast cells in high burden granulomas, we looked for potential direct links between them (**Figure 6**). To understand diversity in plasma cell populations, we first examined the distribution of immunoglobulin heavy chain expression among the plasma cells and detected limited IgE expression. Instead, we observed that the vast majority of plasma cells express either *IGHA* or

IGHG constant chains **(Figure S8),** suggesting that they are the dominant antibody classes induced by Mtb in the granuloma microenvironment.

As the presence and function of mast cells in Mtb lung granulomas has yet to be characterized, we sought to further validate this transcriptional finding (**Figure 2C-D, Figure 6A-B**). To confirm the presence and examine the localization of mast cells in Mtb granulomas, we performed immunohistochemistry on paraffin embedded sections of NHP and human granulomas using Tryptase and C-kit/ CD117 markers by (**Figure 6C-D; STAR* Methods**). This revealed that mast cells primarily localize to the outer regions of the granuloma, including the lymphocyte cuff in NHP (**Figure 6C**), and can be found within and around human granulomas (**Figure 6D**)**.** In our data, mast cells are characterized by expression of *IL-13* **(Figure 6E)**, which we also recently observed in a study of human nasal polyposis (Ordovas-Montanes et al., 2018) and *IL-4* (**Figure 6E**). Moreover, we find that mast cells co-occur with fibroblasts (**Figure 6A, Table S11**), consistent with a wound healing response (Rodrigues et al., 2019; Wong et al., 2020; Wulff and Wilgus, 2013). These data are consistent with a role for mast cells in peripheral fibrosis but might also suggest additional regulatory interactions with lymphocytes which will be the subject of future studies.

Discussion

A classic tenet in TB is that within most infected individuals the immune response is capable of controlling but never fully eliminating infection, and only a small percentage of infected individuals develop active disease (O'Garra et al., 2013). The cynomolgus macaque model of Mtb infection has taught us that the true picture is likely more complex. Within every individual, there are granulomas that represent geographically circumscribed instances of sterilizing immunity, of immune standoff—control but not sterilization—and, at least in some individuals, frank immune failure (Flynn, 2006, 2010; Lin et al., 2014b; Lin et al., 2009). This heterogeneity provides an opportunity to define cellular and molecular factors that correlate with bacterial control in the animal model that best recapitulates human infection and disease (Coleman et al., 2014a) to identify potential prevention and cure strategies for TB.

To enable unbiased investigation of which factors within a granuloma might facilitate bacterial control, we performed high-throughput single-cell transcriptional profiling of 26 granulomas spanning a wide range of bacterial burdens in cynomolgus macaques, while simultaneously tracking granuloma development by PET CT imaging and executing detailed microbiologic quantification. Our data represent the first unbiased single-cell investigation of factors associated dynamically with natural control of Mtb in granulomas. Here, we focused on granulomas at 10 weeks p.i., a key inflection point in Mtb infection where innate and adaptive immune responses are in place. In previous work, we demonstrated that in lesions formed upon infection, viable bacterial burdens are highest at ~4 weeks p.i. and that by ~10 weeks p.i., bacterial burden decreases in many granulomas, with a subset having fully sterilized (Lin et al., 2014b) (**Figure S1**). As we can distinguish low bacterial burdens that occur through sterilization, rather than late or very slow bacterial growth, by measuring cumulative bacterial burden using a genome counting approach (CEQ), our imaging and microbiologic tools provide

a robust means of assessing lesional dynamics. This, in turn, allows us to capture features that associate with, and may be causally involved in, bacterial clearance (low CFU/CEQ).

Our single-cell analysis of granulomas at this pivotal 10 week p.i. time point revealed cellular factors correlated with both immune successes and failures. Consistent with previous observations, our findings reinforce a critical role for T cells in the control of Mtb infection. Nevertheless, given the substantial increase in resolution, our data paint a more nuanced picture, highlighting several subclusters and subpopulations within the larger unified T/NK cell cluster, including Type1-Type 17 hybrid subpopulations, cytotoxic cell subclusters, and stem-like memory T cells, that may play a critical role in bacterial control at the local granuloma level. What became clear through these analyses is that functional phenotypes, rather than canonical lymphocyte cell types, defined the subclusters and were associated with bacterial control, sometimes in a temporal fashion. Moreover, our data reveal several features associated with loss of bacterial control – most notably an increase in both mast and plasma cells in high burden lesions.

Although both CD4 and CD8 T cells have been implicated in control of Mtb infection, the cytotoxic function of lymphocytes in Mtb infection has been relatively understudied, with emphasis placed instead macrophage activating cytokines, such as IFN-γ and TNF. However, subclustering the T/NK cluster revealed six subclusters that are defined by cytotoxic gene expression, each with a different flavor. This is the first study to describe the complexity of cytotoxic cells in granulomas in the context of bacterial burden. These subclusters did not align cleanly with canonical markers of cellular identity that would define them as classical CD8$\alpha\beta$ or CD4 T cells, NK, NK T cells, or $\gamma\delta$ T cells, but instead appear to be variable mixtures of cell types with common transcriptional programming. Of these, cytotoxic cluster 4, which is

enriched in CD8αβ T cells and defined by expression of several granzymes and perforin but only low levels of granulysin, is associated with control of Mtb in granulomas and likely represents cytotoxic effector T cells that target infected cells for apoptosis. Although the other cytotoxic subsets do not correlate with overall control of Mtb in granulomas, temporal analysis of granulomas via PET CT scanning allowed us to identify the early granulomas that form upon infection. In those granulomas, control of early Mtb infection was associated not only with cytotoxic subcluster 4 but also cytotoxic subclusters 1, 2, and 5. These include innate-like CD8+ subsets (NKT, NK, and γδ T cells) with tri-cytotoxic potential (perforin, granzymes, and granulysin) (subcluster 1), granzyme K expressing T cells (subcluster 5) and an interesting population with characteristics of peripheral tolerant T cells (subcluster 2). Subclustering the T1/17 cluster also revealed a cytotoxic T cell subpopulation that was associated with lower bacterial burdens. Together these data point to important and previously underestimated roles for cytotoxic innate and adaptive lymphocytes in temporal control of Mtb in granulomas, and support further study of cytotoxic cells as a potential target for vaccination.

The T1-T17 subcluster of the T and NK cell cluster, characterized by transcriptional patterns associated with both Type 1 and Type 17 T cells, was most strongly associated with overall bacterial control. While a number of studies have implicated lymphocytes with CD4 Th1 and Th17 functionality in the control of Mtb infection (Darrah et al., 2020; Gideon et al., 2015; Lyadova and Panteleev, 2015; Mpande et al., 2018), our scRNA-seq analysis reveals functional characteristics of cells associated with control that do not neatly follow expected T cell ontogenies defined by surface marker staining; rather, cells within express both Type 1 and Type 17 genes and are a mixture of *CD4* and *CD8* expressing T cells. While the T1-T17 subcluster was defined by expression of several transcription factors and surface receptors consistent with Th17 cell differentiation, there was a paucity of expression of either *IL17A* or

628 *IL17F*. Although this could be due to failed detection or a difference between transcription and
629 translation, we previously reported that lymphocytes expressing T1 or T17 cytokines were at
630 relatively low frequencies in granulomas (Gideon et al., 2015). Notably, the T1-T17 subcluster
631 shares many features with previously characterized T cell subsets including Th1* and ex-Th17
632 cells which do not express IL-17 (Acosta-Rodriguez et al., 2007; Basdeo et al., 2017). These
633 subsets, observed previously among CD4 T cells, represent precursors to long lived tissue
634 memory and have been shown to play a crucial protective role in autoimmunity, bacterial control
635 and memory immune responses to pathogens (Amezcua Vesely et al., 2019; Liang et al., 2015;
636 van Hamburg and Tas, 2018; Wacleche et al., 2016). Collectively, this suggests that the T1-
637 T17 population represents a spectrum of tissue-resident effector and effector-memory T cells
638 that arise in response to Mtb infection, and should be considered as targets to be exploited for
639 vaccine development.
640
641 The T1-T17 subcluster consists of both *CD4* and *CD8A/B* expressing cells with shared
642 functional programming but contains subpopulations with unique features. The CD4-enriched
643 subpopulation expresses some of the cluster defining genes associated with the stem-like T cell
644 subcluster, but does not have obvious effector functions. Although exact phenotype of this
645 subpopulation is not yet clear, there is a trend toward association with lower bacterial burden
646 and could represent a T cell population restrained in effector functions and metabolic activity,
647 preventing excessive activation which could lead to detrimental inflammation or exhaustion.
648 The *CD8* T1-T17 subpopulation that associated with control was characterized by expression of
649 cytotoxic effector molecules. Interestingly, most of the *IFNG* and *TNF* expression from the T1-
650 T17 cluster came from a CD4 and CD8 subpopulation that did not associate with overall
651 bacterial control except in early-detected granulomas. However, cytotoxic clusters 1, 2, 4 and 5
652 also show some expression of *IFNG* and *TNF*, and cytotoxic cluster 4 is associated with overall
653 bacterial control. The relatively limited association between expression of these

proinflammatory cytokines and bacterial control may reflect the temporal dynamics that distinguish lesions that have already achieved control versus those in which there is ongoing bacterial growth. In previous flow cytometry-based studies of NHP granulomas, expression of IFN-γ did not correlate with bacterial burden, and other T1/T17 cytokines including TNF, IL-2 and IL-17 only correlated with lower bacterial burden in conjunction with anti-inflammatory cytokines such as IL-10 expressed in the same granuloma.

Our data also revealed an interesting *CD4* and *CD8* expressing T cell cluster associated with control of bacterial burden that resembles stem-like T cells. We hypothesize that these cells may be a source of T cell renewal in granulomas, and may differentiate into the various functional subsets we observe within them. This hypothesis is supported by TCR sharing between the stem-like T cells and the T1/17 or other subclusters in a limited number of granulomas; more extensive TCR coverage will help to solidify this relationship in future studies. Another possibility is that the stem-like T cells represent memory T cells that are not specific for Mtb antigens, but migrate to the granuloma due to inflammatory signals, including chemokines. Indeed, flow cytometry based studies support that a majority of T cells in granulomas do not respond to Mtb antigens by making cytokines nor are they exhausted (Gideon et al., 2015; Sakai et al., 2016; Wong et al., 2018). The stem-like T cells warrant additional study, as they associate with control of Mtb in granulomas and could be explored as a potential vaccine target.

Importantly, to our knowledge, this study is the first to link longitudinal PET-CT imaging and single-cell sequencing data in the context of infectious disease, and this provides novel insights into the temporal evolution of immunologic control in Mtb infection. Interestingly, our imaging and microbiologic analyses revealed a significant relationship between the time at which granulomas are first observed on PET-CT and bacterial burden**.** Granulomas that are observed only on the 10-week scans had consistently lower bacterial burdens, despite having

680 approximately similar cumulative (CEQ) bacterial burdens. These data indicate that late-
681 detected granulomas are not just captured at an earlier stage in their development as a result of
682 dissemination or slower initial growth, but actually demonstrate greater bacterial killing.
683 Focusing on the early-detected, or originally established, granulomas revealed that initial control
684 of infection is significantly associated with cytotoxic functions (both innate and adaptative) as
685 well as T1-T17 subpopulation 3 expressing *IFNG*/*TNF*. These findings solidfy the importance of
686 considering cytotoxic function, not just cytokine function, in vaccine strategies that can prevent
687 Mtb infection.
688
689 The T1-T17 subcluster was expanded primarily in late-detected relative to early-detected
690 lesions and strongly associated with control of Mtb. We hypothesize that these granulomas
691 arise in the context of a more established adaptive immune response and thus harbor a more
692 bactericidal immune ecosystem. Such a model is consistent with recent observations that
693 granulomas established in immune primed environments are better at killing Mtb than those
694 established in a naïve lung – e.g., existing Mtb infection (Cadena et al., 2018) or IV-BCG or
695 intrabronchial BCG vaccination, where Th1/17 expression patterns were observed to correlate
696 with protection (Darrah et al., 2020; Dijkman et al., 2019). Here, we extend these findings by
697 looking at primary infection within an unmanipulated system, linking imaging with scRNA-seq to
698 identify the different paths granulomas may take based on when they arise, and the cells
699 associated with these distinct outcomes. By examining the ecosystem of granulomas over time
700 our data suggest that most T1/T17 cells emerge later in the infection and lead to increased
701 killing of Mtb. Thus, targeting induction of these cells via vaccination could improve early control
702 of infection.
703
704 The immune correlates of failure to control are even more unexpected. Although it has been
705 hypothesized that immune exhaustion may contribute to failed bacterial control (Behar et al.,

2014; Jayaraman et al., 2016; Khan et al., 2017), we do not find associations between classical T cell exhaustion molecules and bacterial burden, which supports previous observations in NHP granulomas (Gideon et al., 2015; Sakai et al., 2016; Wong et al., 2018). Instead, lesions with high bacterial burdens are characterized by significantly higher proportions of plasma and mast cells than those with lower burdens. Notably, while these plasma cells do not appear to be expressing *IgE* (in contrast to *IGHA* and *IGHG),* the mast cells express *IL-13 and IL-4*, suggesting a possible link between the pair (Takeuchi et al., 2015). The expression of *IGHA* and *IGHG* and presence of plasma cells in granulomas support the notion that antibodies may play a prominent role in Mtb infection, perhaps with different effects as a function of antibody quality (Achkar et al., 2015; Jacobs et al., 2016; Lu et al., 2016). Immunohistochemistry confirms the presence of mast cells in TB granulomas in both NHP and humans, where they appear located in and around the lymphocyte cuff, suggesting potential regulatory interactions with T and NK cells or with the macrophages present within this region**.** IL-13 and IL-4 or expression of IL-4Rα (the receptor for these cytokines) have been reported to modulate CD8 T cell function, including inhibition of cytotoxic activity, supporting the potential for mast cells to regulate the T cell responses in granulomas(Kienzle et al., 2005; Wijesundara et al., 2013). While mast cells have been described in granulomatous conditions, such as TB lymphadenitis (Taweevisit and Poumsuk, 2007), leprosy skin lesions (Bagwan et al., 2004), and liver granulomas (Celasun et al., 1992), and may orchestrate immune cross talk in TB (Garcia-Rodriguez et al., 2017), this is the first description of direct correlation with Mtb bacterial burden in individual TB granulomas. While more detailed studies on the roles of mast cells in TB are indicated, this observation provides exciting new avenues to explore the immune architecture of failed immunity in TB lung granulomas, and suggests new intervention strategies. In conjunction with elevated mast and plasma cell frequencies, we also observed higher proportions of fibroblasts in high burden lesions. This may reflect attempts at wound healing (i.e., a canonical type-2 response) in the face of higher bacterial burden, as suggested by other

732 studies (Wong et al., 2020) and uncovers potentially therapeutically relevant intercellular
733 interactions (Rubinchik and Levi-Schaffer, 1994) for future follow up.
734
735 It is important to recognize the limitations in our data. Our TCR sequencing data reveal
736 significant sharing of TCR sequences between granulomas within, but not across, animals. T
737 cells appear to be responding to similar antigens across granulomas, irrespective of bacterial
738 burden, suggesting that the abundance and composition of T cell phenotypes, rather than
739 antigen specificity, is a critical determinant of granuloma-level bacterial control. However, our
740 recovery of CDR3 sequences was relatively low, which limits our ability at this time to go beyond
741 analysis of enriched clones.
742
743 Moreover, the granuloma is an inherently heterogenous environment and includes necrotic
744 debris, requiring robust technical correction and quality control; this results in an analysis of only
745 high-quality cells. Since only a fraction of cells from each granuloma are analyzed, proportions
746 may not reflect the true composition of cells within a granuloma and may be skewed toward
747 lymphocytes highlighting the importance of orthogonal validations. Given cell and granuloma
748 numbers, rare populations, including DURTs, were more difficult to analyze in detail. We
749 focused primarily on cell types, subclusters, and subpopulations that were correlated with
750 bacterial burden in granulomas. While macrophages are clearly an important component of the
751 immune response in TB granulomas, the heterogeneity of the myeloid populations requires
752 further in depth evaluation with additional samples and time points to appreciate which functions
753 and cell types are associated with control or failure. Relatedly, the granuloma landscape
754 investigated here is from a single, albeit pivotal, time point. It is likely that expression of certain
755 genes that occur early in infection and then are downregulated as infection progresses will be
756 missed, as will some populations critical to guiding overall lesional outcome. More generally,
757 matched analyses of earlier and later time points post-infection along with analysis of lung

758 tissue and granulomas from vaccinated or reinfected and protected animals will provide a more
759 complete picture of the temporal control of Mtb in granulomas.
760
761 In summary, our study affords unprecedented, unbiased views of the cellular and molecular
762 features associated with control of Mtb in primary lung granulomas. Beyond recapitulating
763 canonical correlates, our analysis defines nuanced actionable innate and adaptive functional
764 cell states including novel data on cytotoxic subsets, stem-like T cells and T1/17 CD4 and CD8
765 T cells, uncovers a permissive role for cells consistent with type-2 responses (mast and plasma
766 cells) and sheds light on essential dynamics among host-pathogen interactions (Iwasaki and
767 Medzhitov, 2015). Collectively, our data substantiate a model where Mtb burden within early
768 forming lesions is dictated by the interplay among restrictive, inflammatory innate-like responses
769 and permissive, protective type-2 (wound healing) responses seeking to balance bacterial
770 control with the maintenance of essential tissue functionality, respectively. In those lesions
771 forming late, this balance can be tipped by an onslaught of adaptive T1-T17 and cytotoxic
772 responses which are capable of controlling local disease, given sufficient access. Such a
773 framework is consistent with previous observations of natural (Cadena et al., 2018) or induced
774 (Darrah et al., 2020) control, and nominates several discrete putative axes of intra- and
775 intercellular signaling that may prove therapeutically or prophylactically valuable, as well as
776 intellectual links to other inflammatory and infectious diseases that affect epithelial barrier
777 tissues.
778

ACKNOWLEDGEMENTS

We are grateful to the research and veterinary technicians: Chelsea Chedrick, Carolyn Bigbee, Nicholas Schindler, Mark Rogers, Tara Rutledge, Chelsea Causgrove and Brianne Stein in the Flynn lab who assisted with this work, as well as helpful discussions with members of the Flynn, Scanga, Mattila, Lin and Shalek laboratories. We also thank the efforts of the University of Pittsburgh Division of Laboratory Animal Research technicians for husbandry of the animals.

This work was supported in part by the Searle Scholars Program (AKS), the Beckman Young Investigator Program (AKS), a Sloan Fellowship in Chemistry (AKS), the NIH (5U24AI118672, BAA-NIAID-NIHAI201700104) (AKS), and the Bill and Melinda Gates Foundation (OP1139972: AL, SMB, SMF, JLF, AKS). We acknowledge support from the American Lung Association RG571577(HPG), F30-AI143160 (TKH), NIH T32A1065380 (NLG), NSF GRFP grant (SKN 1122374) Wellcome Trust Fellowship award 210662/Z/16/Z (AL), Koch Institute Support (core) grant P30-CA14051 from the National Cancer Institute (CL), NIH CFAR P30 AI060354(BB) NIH R01A1022553 (BB), JR (T32 A1007387).

DECLARATION OF INTEREST

A.K.S. reports compensation for consulting and/or SAB membership from Merck, Honeycomb Biotechnologies, Cellarity, Cogen Therapeutics, Ochre Bio, and Dahlia Biosciences.

CL: shareholder and consultant Honeycomb biotechnologies.

798 ***Figures legends:***

799

800 **Figure 1. Study design, experimental set up, characteristics of animals over the course of**
801 **Mtb infection and granuloma bacterial burden.**

802 **A.** Architecture of macaque TB lung granuloma, where lymphocytes and macrophages are
803 present in distinct regions. Immunohistochemistry and confocal microscopy were
804 performed on a granuloma from an animal at 11 weeks post-Mtb infection to visualize
805 localization of CD11c+ macrophages (cyan), CD3+ T cells (yellow), and CD20+ B cells
806 (magenta).

807 **B.** Study design: Cynomolgus macaques (n=4) were infected with a low-dose inoculum of
808 Mtb (Erdman strain) and serial PET-CT scans were performed at 4, 8, and 10 weeks
809 post-infection with the final scan used as a map for lesion identification at necropsy.
810 Individual granulomas were excised and homogenized. CFU and CEQ assays were
811 performed on all granulomas (top right) and 26 individual granulomas across 4 animals
812 were randomly selected at necropsy for Seq-Well assays (bottom right).

813 **C.** Total lung FDG activity (in log scale) measured by PET scans of each animal at 4, 8 and
814 10-weeks post-Mtb infection showing trajectories of lung inflammation.

815 **D.** Distribution of CFU per granuloma sampled for Seq-Well assay for each animal. Each
816 dot is an individual granuloma.

817 **E.** CFU $\log_{10}$ per granuloma (total live bacteria) organized by tertiles. Each dot is a
818 granuloma. Colors correspond to CFU tertile ranges in E-G: Green: 0-500 CFU, Yellow:
819 500-5000 CFU, and Red: >5000 CFU. Box plot showing median, IQR and range. Kruskal
820 Wallis test with Dunn's multiple testing correction for panels E-G.

821 **F.** CEQ $\log_{10}$ per granuloma (Chromosomal equivalents, CEQ, live + dead Mtb) organized
822 by tertiles. Colors correspond to CFU tertile ranges.

823 **G.** Ratio between CFU (viable bacteria) and CEQ (total bacterial burden) i.e., relative
824 bacterial survival. Lower ratio (negative values) corresponds to increased killing and
825 higher ratio corresponds to increased Mtb survival.

826

827 **Figure 2. Analysis of single-cell sequencing of tuberculosis lung granulomas**.

828 A. UMAP plot of 109,584 cells from 26 granulomas colored by identities of 13 generic cell
829 types.

B. Expression levels of cluster defining genes enriched across 13 generic cell types. Color intensity corresponds to the level of gene expression, while the size of dots represents the percent of cells with non-zero expression in each cluster.

C. Significant correlations between proportion of T/NK cells, mast cells, plasma cells and fibroblasts with bacterial burden of individual granulomas (CFU per granuloma) using non-parametric Spearman's rho correlation test.

D. Relationship between granuloma proportional composition of cell type clusters and CFU in tertiles. Statistics: Kruskal Wallis test with Dunn's multiple testing correction. Adjusted p value for cell type composition comparing low and high tertiles is presented in boxes. Box plot showing median, IQR and range; each dot represents a granuloma. Spearman's Rho and p values are shown in boxes at the top for corresponding cell type clusters.

Figure 3: Diversity in the unified T and NK cell cluster and relationship to granuloma-level bacterial burden.

A. Subclustering 41,222 cells in the unified T/NK cell cluster, colored by subclusters. Subclusters are numbered based the expression patterns.

B. Frequency of expression of TCR genes *TRAC*, *TRBC1* or *TRBC2* (yellow) and *TRDC* (green) across 13 T/NK cell subclusters.

C. Expression levels of T/NK cell cluster-defining genes. Color intensity corresponds to the level of gene expression and the size of dots represents the percent of cells with non-zero expression in each cluster. Y-axis identifies subclusters.

D. Correlations between proportion of T/NK cells and subclusters (1-13) with bacterial burden of individual granulomas (CFU per granuloma) using non-parametric Spearman's rho correlation test. Subclusters with significant negative correlation values are highlighted in blue.

Figure 4: Phenotypic Diversity in T1-T17 cells.

A. T1-T17 subcluster overlaid on unified T/NK cell cluster (left) and colored by normalized expression values for T1-T17 subcluster-defining genes (bold outlined boxes) and non-enriched canonical Type1 and Type 17 genes (right).

B. Subclustering of 9,234 T1-T17 cells resulting in 4 phenotypic sub-populations.

C. Cluster defining genes for T1-T17 subpopulation 1, 2, 3 and 4. Color intensity corresponds to the level of gene expression and the size of dots represents the percent of cells with non-zero expression in each cluster.

D. Subclustering of T1-T17 cells colored by normalized gene expression values for selected subcluster (top row) and sub-population defining genes.

E. Left: Relationship between the T1-T17 sub-populations and granuloma bacterial burden in tertiles. Statistics: Kruskal Wallis test with Dunn's multiple testing correction. Adjusted p value for cell type composition comparing low and high CFU tertiles is in boxes. Box plot showing median, IQR and range; each dot represents a granuloma. **Right:** Correlations between proportion T1-T17 subcluster and subpopulation 1-3 with bacterial burden of individual granulomas (CFU per granuloma) using non-parametric Spearman's rho correlation test.

Figure 5. Association of cell type proportions with timing of granuloma formation

A-C. CFU $\log_{10}$ values(A), CEQ $\log_{10}$ values (B) and relative bacterial survival (CFU/CEQ)(C) for granulomas grouped by time of initial observation by PET-CT imaging. Early detection (yellow): those identified at 4 weeks p.i.; Late detection (green): those identified at 10 week p.i..

D,E. Canonical cell type clusters (D) and T/NK subclusters (E) that are significantly different between early and late detection granulomas. See Table S10 for full data.

F. Early (4 week) detection granulomas comparing lowest CFU (n=6) and highest CFU (n=6) granulomas.

G, H. Relationship between the abundance of canonical cell types (G) and T/NK subclusters (H) with bacterial burdens among low CFU and high CFU early-detected granulomas. Each dot represents a granuloma. Box plot shows median, IQR and range. Statistics: non-parametric Mann Whitney U test. See Table S10 for full data

Figure 6: Cellular ecosystem in TB lung granulomas

A. Pairwise Pearson correlation values proportions of canonical cell types and T/NK and macrophage subclusters across 26 granulomas. Hierarchical clustering of correlation coefficients identified 5 groups (indicated by color) of cell types with correlated abundance in granulomas.

B. Relationship between the distribution of correlated cell-types between high and low CFU granulomas (left), and across all 26 granulomas ordered from lowest CFU (left) to

highest CFU (right). Colored boxes indicate granuloma CFU range by green boxes (low), orange boxes (mid) and maroon boxes (high); which granulomas came from which animal by salmon boxes (3817), yellow boxes (3917), Navy blue boxes (4017) and 4217 boxes (light blue) and time of detection is indicated by yellow boxes (10 weeks) and green boxes (4 weeks).

C. Detection of mast cells in a 10-week NHP granuloma using immunohistochemistry, staining for tryptase (green) and c-kit (CD117)(red).

D. Detection of mast cells in a human lung granuloma. Hematoxylin and eosin stain and immunohistochemistry with multinucleated giant cells (stars, (top left) and c-kit (CD117) staining (indicated by arrows, top and bottom right).

E. Left: UMAP plot of 109,584 cells from 26 granulomas colored by identities of 13 generic cell types. **Right:** expression levels of IL-13 and IL-4 genes overlaid on UMAP plot of 109,584 cells.

Supplemental figures:

Figure S1: CFU per granuloma decreases over time.

A. Each column depicts the CFU for all granulomas of an individual macaque (N=88 macaques), ranging from 4 weeks to 17 weeks post-infection. Each dot represents a granuloma. Lines are at means (per animal) and different colors represent weeks post-infection.

B. CFU per granuloma decreases significantly starting at 10-11 weeks post-infection. Each dot represents the mean CFU per granuloma of an individual animal, with the x-axis indicating weeks post-infection at which necropsy was performed. Lines are at medians. Differences between time points were tested using Kruskal-Wallis test with Dunn's multiple comparison adjustment. (* $p < 0.05$, ** $p < 0.01$, *** $p < 0.001$, **** $p < 0.0001$.)

Figure S2: Sequencing, alignment and QC pipeline (see STAR* methods)

A, D, I. Array-specific processing pipeline.

B. Array specific Louvain clustering (Resolution = 1.25).

C. Cluster-defining gene expression was determined within each array.

E. Overview of Cluster-Specific Summary Score.

F. Estimation of soup-thresholds for correction of ambient RNA contamination. Left: Relationship between soup-thresholds (x-axis) the number of soup defining genes detected for each array (y-axis). Right: Relationship between soup-thresholds (x-axis) and the cumulative proportion of soup-defining gene expression (y-axis).

G. Hierarchical clustering results used to identify and remove clusters defined by ambient contamination from each array.

H. t-SNE plot showing removal of clusters characterized as ambient RNA.

J. Estimation of array-specific contamination rates using SoupX.

K. Identification and removal of array-specific doublets.

Figure S3: Identification of Canonical Cell Types.

A. Waterfall plot showing stability of cell-type clusters at multiple clustering resolutions. Boxed row (resolution=1.00) selected for downstream analysis.

B, C Distribution of lung cell-type signatures obtained from the Tabula muris (B) and Mouse cell (C) atlas.

D. UMAP plot of 109,584 cells colored by Louvain clusters (resolution = 1.00).

F. Waterfall plot showing the stability of sub-clustering analysis of 3,123 cells with a proliferating gene signature.

G. Distribution of canonical cell type signatures across subclusters of proliferating cells.

H. UMAP plot of 109,584 cells colored by 13 canonical cell type clusters.

I. Expression levels of cluster-defining genes overlaid on UMAP plot in panel G.

J. Correlations between bacterial burden and abundance of each canonical cell type cluster. Correlation was calculated using non-parametric Spearman's rho test.

Figure S4. Macrophage heterogeneity in Mtb granulomas.

A. Waterfall plot showing the stability of macrophage sub-clusters. Boxed row (resolution=0.55) selected for downstream analysis.

B. UMAP plot of 27,670 macrophage cluster colored by phenotypes.

C. Cluster-defining genes across macrophage subclusters.

D. Macrophage subcluster-defining genes overlaid on macrophage plot in panel B.

E. Boxplots showing bacterial burden in tertiles and composition of macrophage sub-populations. Box plot showing median, IQR and range; each dot represents a granuloma. Kruskal Wallis test with Dunn's multiple testing correction. The only significant value is for Macrophage subcluster 3 between low and high CFU tertiles

p=0.0004). Spearman's Rho and p values are shown in boxes at the top for corresponding macrophage subclusters.

Figure S5. Sub-clustering and phenotypic identification of T/NK cell populations

A. Waterfall plot showing the stability of T/NK cell sub-clustering. Boxed row (resolution=0.55) selected for downstream analysis.

B. UMAP plot of 44,766 T/NK cells with a sub-cluster of 3,544 T/NK cells defined by residual contamination highlighted (blue).

C. Waterfall plot showing the stability of T/NK cell sub-clustering following removal of contaminated T cell sub-cluster. Boxed row (resolution=0.75) selected for downstream analysis.

D. T/NK subclustering UMAP overlaid with normalized gene expression for CD4, CD8A, and CD8B (top). Expression of these genes across 13 sub-clusters (bottom) where color intensity corresponds to level of gene expression and size of dots represents the percent of cells with non-zero expression in each cluster.

E. Frequency of expression of *CD4* (blue), *CD8A* and/ *CD8B* (green), *CD4* and *CD8A/B* (orange) or no expression of *CD4/CD8A/B* (yellow) across 13 T/NK cell subclusters.

F. UMAP plots overlaid with normalized expression levels for selected T/NK cell subcluster-defining genes.

Figure S6: TCR repertoires in granulomas

A. UMAP plots of 41,222 T/NK cells colored by recovery of TCR CDR3 sequences

B. Fraction of each T/NK sub-cluster with recovery of TCR CDR3 sequences

C. Enrichment of TCR-alpha (Alpha-CDR3 >= 10 cells, left), TCR-beta (Beta-CDR3 >= 12 cells, middle), and both TCR-alpha and TCR-beta (Alpha-Beta-CDR3 >= 12 cells, right) in the unified T/NK cluster.

D. Fraction of each T/NK sub-cluster enriched for TCR-alpha (red), TCR-beta (blue), and TCR-alpha and TCR-beta (green) sequences.

E. Sharing of enriched TCR sequences across all granulomas. Colors above heatmaps correspond to animal and CFU tertiles. Individual heatmaps are shown for TCR-alpha (Alpha-CDR3 >= 10 cells, left), TCR-beta (Beta-CDR3 >= 12 cells, middle), and TCR-Alpha/Beta (Alpha-Beta CDR3 >= 10 cells, right).

F. Distribution of T/NK cell subclusters within enriched alpha-beta TCR clones across all animals.

G. Distribution of T/NK cell subclusters within enriched alpha-beta TCR clones between high and low burden lesions within Animal 4017.

H. UMAP plots of 41,222 T/NK cells colored by detection of TRAJ TRAV TCR sequences (MAIT: genes , iNKT (genes), and GEM (genes).

Figure S7 Late detection granulomas have lower CFU than early detection granulomas.

A. CFU per granuloma is shown for early detection (blue) and late detection (red) within each animal. Box plots lines represent the median, IQR and range Each dot represents a granuloma.

B. CFU is significantly lower in new granulomas within animals. Each dot (and line) represents the median CFU per granuloma of each animal. Statistics: paired t-test .

Figure S8. Expression of selected functional transcripts.

A. Expression levels of select functional genes overlaid on UMAP plot of 109,584 cells.

B. UMAP plot of 109,584 cells from 26 granulomas colored by identities of 13 generic cell types.

Supplemental Table legends:

Table S1: Granuloma CFU, CEQ , CFU/CEQ; PET-CT: SUV-R, Size and Time of detection

Table S2a: Seq-Well array loading densities and doublet rate

Table S2b: Technical correction data: SoupX

Table S2c: Doublet removal Metadata

Table S2d: Cell level metadata

Tablet S3: Canonical cell type enrichment gene list: 13 cell type clusters

Table S4: Cells type composition: percentage of assigned granuloma cells. A) canonical cell type clusters, b)macrophage subclusters, c) T/NK subclusters and d) T1T17 subpopulation

Tablet S5: Macrophage subcluster enrichment:9 subclusters

Table S6: T/NK subclustering: enrichment gene list :13 T/NK subclusters

Table S7:Type1-Type-17 subpopulation enrichment

Table S8: Correlation (Spearman's rho) with bacterial burden and difference between in percentage of cells between low and high CFU tertiles (Kruskal-Wallis Test with Dunn's multiple testing correction): A) canonical cell type clusters, b) T/NK subclusters and C) T1T17 subpopulation

Table S9: TCR repertoires

Table S10: Difference in cellular abundance and association with bacterial burden. (a) Early detection and late detection granulomas, (b)Early detection granulomas

Table S11: Cellular ecology

Table S12: Association of cell group abundance with bacterial burden : (1) All: CFU low vs high, (2) Early detection: CFU: lowest vs highest and timing of granuloma detection (Early vs late)**.**

References:

Achkar, J.M., Chan, J., and Casadevall, A. (2015). B cells and antibodies in the defense against Mycobacterium tuberculosis infection. Immunol Rev *264*, 167-181.

Acosta-Rodriguez, E.V., Rivino, L., Geginat, J., Jarrossay, D., Gattorno, M., Lanzavecchia, A., Sallusto, F., and Napolitani, G. (2007). Surface phenotype and antigenic specificity of human interleukin 17-producing T helper memory cells. Nat Immunol *8*, 639-646.

Ahmed, R., Roger, L., Costa Del Amo, P., Miners, K.L., Jones, R.E., Boelen, L., Fali, T., Elemans, M., Zhang, Y., Appay, V.*, et al.* (2016). Human Stem Cell-like Memory T Cells Are Maintained in a State of Dynamic Flux. Cell Rep *17*, 2811-2818.

Algood, H.M., Lin, P.L., and Flynn, J.L. (2005). Tumor necrosis factor and chemokine interactions in the formation and maintenance of granulomas in tuberculosis. Clin Infect Dis *41 Suppl 3*, S189-193.

Amezcua Vesely, M.C., Pallis, P., Bielecki, P., Low, J.S., Zhao, J., Harman, C.C.D., Kroehling, L., Jackson, R., Bailis, W., Licona-Limon, P.*, et al.* (2019). Effector TH17 Cells Give Rise to Long-Lived TRM Cells that Are Essential for an Immediate Response against Bacterial Infection. Cell *178*, 1176-1188 e1115.

Ando, M., Ito, M., Srirat, T., Kondo, T., and Yoshimura, A. (2020). Memory T cell, exhaustion, and tumor immunity. Immunol Med *43*, 1-9.

Ardain, A., Domingo-Gonzalez, R., Das, S., Kazer, S.W., Howard, N.C., Singh, A., Ahmed, M., Nhamoyebonde, S., Rangel-Moreno, J., Ogongo, P.*, et al.* (2019). Group 3 innate lymphoid cells mediate early protective immunity against tuberculosis. Nature *570*, 528-532.

Arora, P., Foster, E.L., and Porcelli, S.A. (2013). CD1d and natural killer T cells in immunity to Mycobacterium tuberculosis. Adv Exp Med Biol *783*, 199-223.

Bagwan, I.N., Khandekar, M.M., Kadam, P., Jadhav, M.V., and Deshmukh, S.D. (2004). A study of mast cells in granulomatous lesions of skin, with special emphasis on leprosy. Indian J Lepr *76*, 31-37.

Balin, S.J., Pellegrini, M., Klechevsky, E., Won, S.T., Weiss, D.I., Choi, A.W., Hakimian, J., Lu, J., Ochoa, M.T., Bloom, B.R.*, et al.* (2018). Human antimicrobial cytotoxic T lymphocytes, defined by NK receptors and antimicrobial proteins, kill intracellular bacteria. Sci Immunol *3*.

Basdeo, S.A., Cluxton, D., Sulaimani, J., Moran, B., Canavan, M., Orr, C., Veale, D.J., Fearon, U., and Fletcher, J.M. (2017). Ex-Th17 (Nonclassical Th1) Cells Are Functionally Distinct from Classical Th1 and Th17 Cells and Are Not Constrained by Regulatory T Cells. J Immunol *198*, 2249-2259.

1078 Behar, S.M., Carpenter, S.M., Booty, M.G., Barber, D.L., and Jayaraman, P. (2014).
1079 Orchestration of pulmonary T cell immunity during Mycobacterium tuberculosis
1080 infection: immunity interruptus. Semin Immunol *26*, 559-577.

1081 Brummelman, J., Mazza, E.M.C., Alvisi, G., Colombo, F.S., Grilli, A., Mikulak, J.,
1082 Mavilio, D., Alloisio, M., Ferrari, F., Lopci, E.*, et al.* (2018). High-dimensional single cell
1083 analysis identifies stem-like cytotoxic CD8(+) T cells infiltrating human tumors. J Exp
1084 Med *215*, 2520-2535.

1085 Burel, J.G., Lindestam Arlehamn, C.S., Khan, N., Seumois, G., Greenbaum, J.A.,
1086 Taplitz, R., Gilman, R.H., Saito, M., Vijayanand, P., Sette, A.*, et al.* (2018).
1087 Transcriptomic Analysis of CD4(+) T Cells Reveals Novel Immune Signatures of Latent
1088 Tuberculosis. J Immunol *200*, 3283-3290.

1089 Caccamo, N., Joosten, S.A., Ottenhoff, T.H.M., and Dieli, F. (2018). Atypical Human
1090 Effector/Memory CD4(+) T Cells With a Naive-Like Phenotype. Front Immunol *9*, 2832.

1091 Cadena, A.M., Flynn, J.L., and Fortune, S.M. (2016). The Importance of First
1092 Impressions: Early Events in Mycobacterium tuberculosis Infection Influence Outcome.
1093 mBio *7*, e00342-00316.

1094 Cadena, A.M., Hopkins, F.F., Maiello, P., Carey, A.F., Wong, E.A., Martin, C.J., Gideon,
1095 H.P., DiFazio, R.M., Andersen, P., Lin, P.L.*, et al.* (2018). Concurrent infection with
1096 Mycobacterium tuberculosis confers robust protection against secondary infection in
1097 macaques. PLoS Pathog *14*, e1007305.

1098 Canetti, G. (1955). The tubercle bacillus in the pulmonary lesion of man:
1099 histobacteriology and its bearing on the therapy of pulmonary tuberculosis. Springer.

1100 Cartwright, E.K., Palesch, D., Mavigner, M., Paiardini, M., Chahroudi, A., and Silvestri,
1101 G. (2016). Initiation of Antiretroviral Therapy Restores CD4+ T Memory Stem Cell
1102 Homeostasis in Simian Immunodeficiency Virus-Infected Macaques. J Virol *90*, 6699-
1103 6708.

1104 Celasun, B., Crow, J., and Scheuer, P.J. (1992). Mast cells in granulomatous liver
1105 disease. Pathol Res Pract *188*, 97-100.

1106 Chackerian, A., Alt, J., Perera, V., and Behar, S.M. (2002). Activation of NKT cells
1107 protects mice from tuberculosis. Infect Immun *70*, 6302-6309.

1108 Chancellor, A., White, A., Tocheva, A.S., Fenn, J.R., Dennis, M., Tezera, L., Singhania,
1109 A., Elliott, T., Tebruegge, M., Elkington, P.*, et al.* (2017). Quantitative and qualitative
1110 iNKT repertoire associations with disease susceptibility and outcome in macaque
1111 tuberculosis infection. Tuberculosis (Edinb) *105*, 86-95.

1112 Chen, C.Y., Huang, D., Wang, R.C., Shen, L., Zeng, G., Yao, S., Shen, Y., Halliday, L.,
1113 Fortman, J., McAllister, M.*, et al.* (2009). A critical role for CD8 T cells in a nonhuman
1114 primate model of tuberculosis. PLoS Pathog *5*, e1000392.

1115 Coleman, M.T., Chen, R.Y., Lee, M., Lin, P.L., Dodd, L.E., Maiello, P., Via, L.E., Kim,
1116 Y., Marriner, G., Dartois, V.*, et al.* (2014a). PET/CT imaging reveals a therapeutic
1117 response to oxazolidinones in macaques and humans with tuberculosis. Sci Transl Med
1118 *6*, 265ra167.

1119 Coleman, M.T., Maiello, P., Tomko, J., Frye, L.J., Fillmore, D., Janssen, C., Klein, E.,
1120 and Lin, P.L. (2014b). Early Changes by (18)Fluorodeoxyglucose positron emission
1121 tomography coregistered with computed tomography predict outcome after
1122 Mycobacterium tuberculosis infection in cynomolgus macaques. Infect Immun *82*, 2400-
1123 2404.

1124 Darrah, P.A., Zeppa, J.J., Maiello, P., Hackney, J.A., Wadsworth, M.H., 2nd, Hughes,
1125 T.K., Pokkali, S., Swanson, P.A., 2nd, Grant, N.L., Rodgers, M.A.*, et al.* (2020).
1126 Prevention of tuberculosis in macaques after intravenous BCG immunization. Nature
1127 *577*, 95-102.

1128 Diedrich, C.R., Rutledge, T., Maiello, P., Baranowski, T.M., White, A.G., Borish, H.J.,
1129 Karell, P., Hopkins, F., Brown, J., Fortune, S.M.*, et al.* (2020). SIV and Mycobacterium
1130 tuberculosis synergy within the granuloma accelerates the reactivation pattern of latent
1131 tuberculosis. bioRxiv.

1132 Dijkman, K., Sombroek, C.C., Vervenne, R.A.W., Hofman, S.O., Boot, C., Remarque,
1133 E.J., Kocken, C.H.M., Ottenhoff, T.H.M., Kondova, I., Khayum, M.A.*, et al.* (2019).
1134 Prevention of tuberculosis infection and disease by local BCG in repeatedly exposed
1135 rhesus macaques. Nat Med *25*, 255-262.

1136 Ehlers, S., and Schaible, U.E. (2012). The granuloma in tuberculosis: dynamics of a
1137 host-pathogen collusion. Front Immunol *3*, 411.

1138 Fan, X., and Rudensky, A.Y. (2016). Hallmarks of Tissue-Resident Lymphocytes. Cell
1139 *164*, 1198-1211.

1140 Flynn, J.L. (2006). Lessons from experimental Mycobacterium tuberculosis infections.
1141 Microbes Infect *8*, 1179-1188.

1142 Flynn, J.L., Capuano, S.V., Croix, D., Pawar, S., Myers, A., Zinovik, A., and Klein, E.
1143 (2003). Non-human primates: a model for tuberculosis research. Tuberculosis (Edinb)
1144 *83*, 116-118.

1145 Flynn, J.L., Gideon, H.P., Mattila, J.T., and Lin, P.L. (2015). Immunology studies in non-
1146 human primate models of tuberculosis. Immunol Rev *264*, 60-73.

1147 Flynn, J.L., Klein, E., (2010). Pulmonary Tuberculosis in Monkeys. A Color Atlas of
1148 Comparative Pathology of Pulmonary Tuberculosis, 83-105.

1149 Foreman, T.W., Mehra, S., LoBato, D.N., Malek, A., Alvarez, X., Golden, N.A., Bucsan,
1150 A.N., Didier, P.J., Doyle-Meyers, L.A., Russell-Lodrigue, K.E.*, et al.* (2016). CD4+ T-

cell-independent mechanisms suppress reactivation of latent tuberculosis in a macaque model of HIV coinfection. Proc Natl Acad Sci U S A *113*, E5636-5644.

Fuertes Marraco, S.A., Soneson, C., Delorenzi, M., and Speiser, D.E. (2015). Genome-wide RNA profiling of long-lasting stem cell-like memory CD8 T cells induced by Yellow Fever vaccination in humans. Genom Data *5*, 297-301.

Garcia-Rodriguez, K.M., Goenka, A., Alonso-Rasgado, M.T., Hernandez-Pando, R., and Bulfone-Paus, S. (2017). The Role of Mast Cells in Tuberculosis: Orchestrating Innate Immune Crosstalk? Front Immunol *8*, 1290.

Gattinoni, L., Lugli, E., Ji, Y., Pos, Z., Paulos, C.M., Quigley, M.F., Almeida, J.R., Gostick, E., Yu, Z., Carpenito, C.*, et al.* (2011). A human memory T cell subset with stem cell-like properties. Nat Med *17*, 1290-1297.

Gideon, H.P., Phuah, J., Junecko, B.A., and Mattila, J.T. (2019). Neutrophils express pro- and anti-inflammatory cytokines in granulomas from Mycobacterium tuberculosis-infected cynomolgus macaques. Mucosal Immunol *12*, 1370-1381.

Gideon, H.P., Phuah, J., Myers, A.J., Bryson, B.D., Rodgers, M.A., Coleman, M.T., Maiello, P., Rutledge, T., Marino, S., Fortune, S.M.*, et al.* (2015). Variability in tuberculosis granuloma T cell responses exists, but a balance of pro- and anti-inflammatory cytokines is associated with sterilization. PLoS Pathog *11*, e1004603.

Gierahn, T.M., Wadsworth, M.H., 2nd, Hughes, T.K., Bryson, B.D., Butler, A., Satija, R., Fortune, S., Love, J.C., and Shalek, A.K. (2017). Seq-Well: portable, low-cost RNA sequencing of single cells at high throughput. Nat Methods *14*, 395-398.

Green, A.M., Difazio, R., and Flynn, J.L. (2013). IFN-gamma from CD4 T cells is essential for host survival and enhances CD8 T cell function during Mycobacterium tuberculosis infection. J Immunol *190*, 270-277.

Guo, Y., Chen, J., Shi, L., and Fan, Z. (2010). Valosin-containing protein cleavage by granzyme K accelerates an endoplasmic reticulum stress leading to caspase-independent cytotoxicity of target tumor cells. J Immunol *185*, 5348-5359.

Han, X., Wang, R., Zhou, Y., Fei, L., Sun, H., Lai, S., Saadatpour, A., Zhou, Z., Chen, H., Ye, F.*, et al.* (2018). Mapping the Mouse Cell Atlas by Microwell-Seq. Cell *173*, 1307.

Hirota, K., Yoshitomi, H., Hashimoto, M., Maeda, S., Teradaira, S., Sugimoto, N., Yamaguchi, T., Nomura, T., Ito, H., Nakamura, T.*, et al.* (2007). Preferential recruitment of CCR6-expressing Th17 cells to inflamed joints via CCL20 in rheumatoid arthritis and its animal model. J Exp Med *204*, 2803-2812.

Hovestadt, V., Smith, K.S., Bihannic, L., Filbin, M.G., Shaw, M.L., Baumgartner, A., DeWitt, J.C., Groves, A., Mayr, L., Weisman, H.R.*, et al.* (2019). Resolving medulloblastoma cellular architecture by single-cell genomics. Nature *572*, 74-79.

1188 Hu, S., Lv, P., Yan, Z., and Wen, B. (2019). Disruption of nuclear speckles reduces
1189 chromatin interactions in active compartments. Epigenetics Chromatin *12*, 43.

1190 Huang, H., Sikora, M.J., Islam, S., Chowdhury, R.R., Chien, Y.H., Scriba, T.J., Davis,
1191 M.M., and Steinmetz, L.M. (2019). Select sequencing of clonally expanded CD8(+) T
1192 cells reveals limits to clonal expansion. Proc Natl Acad Sci U S A *116*, 8995-9001.

1193 Hunter, R.L. (2011). Pathology of post primary tuberculosis of the lung: an illustrated
1194 critical review. Tuberculosis (Edinb) *91*, 497-509.

1195 Hunter, R.L. (2016). Tuberculosis as a three-act play: A new paradigm for the
1196 pathogenesis of pulmonary tuberculosis. Tuberculosis (Edinb) *97*, 8-17.

1197 Huynh, J.P., Lin, C.C., Kimmey, J.M., Jarjour, N.N., Schwarzkopf, E.A., Bradstreet,
1198 T.R., Shchukina, I., Shpynov, O., Weaver, C.T., Taneja, R.*, et al.* (2018). Bhlhe40 is an
1199 essential repressor of IL-10 during Mycobacterium tuberculosis infection. J Exp Med
1200 *215*, 1823-1838.

1201 Ivanov, II, McKenzie, B.S., Zhou, L., Tadokoro, C.E., Lepelley, A., Lafaille, J.J., Cua,
1202 D.J., and Littman, D.R. (2006). The orphan nuclear receptor RORgammat directs the
1203 differentiation program of proinflammatory IL-17+ T helper cells. Cell *126*, 1121-1133.

1204 Iwasaki, A., and Medzhitov, R. (2015). Control of adaptive immunity by the innate
1205 immune system. Nat Immunol *16*, 343-353.

1206 Jacobs, A.J., Mongkolsapaya, J., Screaton, G.R., McShane, H., and Wilkinson, R.J.
1207 (2016). Antibodies and tuberculosis. Tuberculosis (Edinb) *101*, 102-113.

1208 Jayaraman, P., Jacques, M.K., Zhu, C., Steblenko, K.M., Stowell, B.L., Madi, A.,
1209 Anderson, A.C., Kuchroo, V.K., and Behar, S.M. (2016). TIM3 Mediates T Cell
1210 Exhaustion during Mycobacterium tuberculosis Infection. PLoS Pathog *12*, e1005490.

1211 Joosten, S.A., Ottenhoff, T.H.M., Lewinsohn, D.M., Hoft, D.F., Moody, D.B., Seshadri,
1212 C., Collaboration for Tuberculosis Vaccine Discovery - Donor-Unrestricted T-cells
1213 Working Group, B., and Melinda Gates, F. (2019). Harnessing donor unrestricted T-cells
1214 for new vaccines against tuberculosis. Vaccine *37*, 3022-3030.

1215 Kazer, S.W., Aicher, T.P., Muema, D.M., Carroll, S.L., Ordovas-Montanes, J., Miao,
1216 V.N., Tu, A.A., Ziegler, C.G.K., Nyquist, S.K., Wong, E.B.*, et al.* (2020). Integrated
1217 single-cell analysis of multicellular immune dynamics during hyperacute HIV-1 infection.
1218 Nat Med *26*, 511-518.

1219 Khader, S.A., Bell, G.K., Pearl, J.E., Fountain, J.J., Rangel-Moreno, J., Cilley, G.E.,
1220 Shen, F., Eaton, S.M., Gaffen, S.L., Swain, S.L.*, et al.* (2007). IL-23 and IL-17 in the
1221 establishment of protective pulmonary CD4+ T cell responses after vaccination and
1222 during Mycobacterium tuberculosis challenge. Nat Immunol *8*, 369-377.

1223 Khader, S.A., and Gopal, R. (2010). IL-17 in protective immunity to intracellular
1224 pathogens. Virulence *1*, 423-427.

1225 Khan, N., Vidyarthi, A., Amir, M., Mushtaq, K., and Agrewala, J.N. (2017). T-cell
1226 exhaustion in tuberculosis: pitfalls and prospects. Crit Rev Microbiol *43*, 133-141.

1227 Kienzle, N., Olver, S., Buttigieg, K., Groves, P., Janas, M.L., Baz, A., and Kelso, A.
1228 (2005). Progressive differentiation and commitment of CD8+ T cells to a poorly cytolytic
1229 CD8low phenotype in the presence of IL-4. J Immunol *174*, 2021-2029.

1230 Kobayashi, T., Okamoto, S., Hisamatsu, T., Kamada, N., Chinen, H., Saito, R.,
1231 Kitazume, M.T., Nakazawa, A., Sugita, A., Koganei, K.*, et al.* (2008). IL23 differentially
1232 regulates the Th1/Th17 balance in ulcerative colitis and Crohn's disease. Gut *57*, 1682-
1233 1689.

1234 Langermans, J.A., Andersen, P., van Soolingen, D., Vervenne, R.A., Frost, P.A., van
1235 der Laan, T., van Pinxteren, L.A., van den Hombergh, J., Kroon, S., Peekel, I.*, et al.*
1236 (2001). Divergent effect of bacillus Calmette-Guerin (BCG) vaccination on
1237 Mycobacterium tuberculosis infection in highly related macaque species: implications for
1238 primate models in tuberculosis vaccine research. Proc Natl Acad Sci U S A *98*, 11497-
1239 11502.

1240 Lenaerts, A., Barry, C.E., 3rd, and Dartois, V. (2015). Heterogeneity in tuberculosis
1241 pathology, microenvironments and therapeutic responses. Immunol Rev *264*, 288-307.

1242 Liang, Y., Pan, H.F., and Ye, D.Q. (2015). Tc17 Cells in Immunity and Systemic
1243 Autoimmunity. Int Rev Immunol *34*, 318-331.

1244 Lin, C.C., Bradstreet, T.R., Schwarzkopf, E.A., Jarjour, N.N., Chou, C., Archambault,
1245 A.S., Sim, J., Zinselmeyer, B.H., Carrero, J.A., Wu, G.F.*, et al.* (2016). IL-1-induced
1246 Bhlhe40 identifies pathogenic T helper cells in a model of autoimmune
1247 neuroinflammation. J Exp Med *213*, 251-271.

1248 Lin, C.C., Bradstreet, T.R., Schwarzkopf, E.A., Sim, J., Carrero, J.A., Chou, C., Cook,
1249 L.E., Egawa, T., Taneja, R., Murphy, T.L.*, et al.* (2014a). Bhlhe40 controls cytokine
1250 production by T cells and is essential for pathogenicity in autoimmune
1251 neuroinflammation. Nat Commun *5*, 3551.

1252 Lin, P.L., Coleman, T., Carney, J.P., Lopresti, B.J., Tomko, J., Fillmore, D., Dartois, V.,
1253 Scanga, C., Frye, L.J., Janssen, C.*, et al.* (2013). Radiologic Responses in Cynomolgus
1254 Macaques for Assessing Tuberculosis Chemotherapy Regimens. Antimicrob Agents
1255 Chemother *57*, 4237-4244.

1256 Lin, P.L., and Flynn, J.L. (2015). CD8 T cells and Mycobacterium tuberculosis infection.
1257 Semin Immunopathol *37*, 239-249.

1258 Lin, P.L., Ford, C.B., Coleman, M.T., Myers, A.J., Gawande, R., Ioerger, T., Sacchettini,
1259 J., Fortune, S.M., and Flynn, J.L. (2014b). Sterilization of granulomas is common in

active and latent tuberculosis despite within-host variability in bacterial killing. Nat Med *20*, 75-79.

Lin, P.L., Myers, A., Smith, L., Bigbee, C., Bigbee, M., Fuhrman, C., Grieser, H., Chiosea, I., Voitenek, N.N., Capuano, S.V.*, et al.* (2010). Tumor necrosis factor neutralization results in disseminated disease in acute and latent Mycobacterium tuberculosis infection with normal granuloma structure in a cynomolgus macaque model. Arthritis Rheum *62*, 340-350.

Lin, P.L., Pawar, S., Myers, A., Pegu, A., Fuhrman, C., Reinhart, T.A., Capuano, S.V., Klein, E., and Flynn, J.L. (2006). Early events in Mycobacterium tuberculosis infection in cynomolgus macaques. Infect Immun *74*, 3790-3803.

Lin, P.L., Plessner, H.L., Voitenok, N.N., and Flynn, J.L. (2007). Tumor necrosis factor and tuberculosis. J Investig Dermatol Symp Proc *12*, 22-25.

Lin, P.L., Rodgers, M., Smith, L., Bigbee, M., Myers, A., Bigbee, C., Chiosea, I., Capuano, S.V., Fuhrman, C., Klein, E.*, et al.* (2009). Quantitative comparison of active and latent tuberculosis in the cynomolgus macaque model. Infect Immun *77*, 4631-4642.

Lin, P.L., Rutledge, T., Green, A.M., Bigbee, M., Fuhrman, C., Klein, E., and Flynn, J.L. (2012). CD4 T cell depletion exacerbates acute Mycobacterium tuberculosis while reactivation of latent infection is dependent on severity of tissue depletion in cynomolgus macaques. AIDS Res Hum Retroviruses *28*, 1693-1702.

Lopez, D., Montoya, D., Ambrose, M., Lam, L., Briscoe, L., Adams, C., Modlin, R.L., and Pellegrini, M. (2017). SaVanT: a web-based tool for the sample-level visualization of molecular signatures in gene expression profiles. BMC Genomics *18*, 824.

Lu, L.L., Chung, A.W., Rosebrock, T.R., Ghebremichael, M., Yu, W.H., Grace, P.S., Schoen, M.K., Tafesse, F., Martin, C., Leung, V.*, et al.* (2016). A Functional Role for Antibodies in Tuberculosis. Cell *167*, 433-443 e414.

Lyadova, I.V., and Panteleev, A.V. (2015). Th1 and Th17 Cells in Tuberculosis: Protection, Pathology, and Biomarkers. Mediators Inflamm *2015*, 854507.

Maiello, P., DiFazio, R.M., Cadena, A.M., Rodgers, M.A., Lin, P.L., Scanga, C.A., and Flynn, J.L. (2018). Rhesus Macaques Are More Susceptible to Progressive Tuberculosis than Cynomolgus Macaques: a Quantitative Comparison. Infect Immun *86*.

Malherbe, S.T., Shenai, S., Ronacher, K., Loxton, A.G., Dolganov, G., Kriel, M., Van, T., Chen, R.Y., Warwick, J., Via, L.E.*, et al.* (2016). Persisting positron emission tomography lesion activity and Mycobacterium tuberculosis mRNA after tuberculosis cure. Nat Med *22*, 1094-1100.

1296 Martin, C.J., Cadena, A.M., Leung, V.W., Lin, P.L., Maiello, P., Hicks, N., Chase, M.R.,
1297 Flynn, J.L., and Fortune, S.M. (2017). Digitally Barcoding Mycobacterium tuberculosis
1298 Reveals In Vivo Infection Dynamics in the Macaque Model of Tuberculosis. mBio *8*.

1299 Mateus, J., Lasso, P., Pavia, P., Rosas, F., Roa, N., Valencia-Hernandez, C.A.,
1300 Gonzalez, J.M., Puerta, C.J., and Cuellar, A. (2015). Low frequency of circulating CD8+
1301 T stem cell memory cells in chronic chagasic patients with severe forms of the disease.
1302 PLoS Negl Trop Dis *9*, e3432.

1303 Mattila, J.T., Diedrich, C.R., Lin, P.L., Phuah, J., and Flynn, J.L. (2011). Simian
1304 immunodeficiency virus-induced changes in T cell cytokine responses in cynomolgus
1305 macaques with latent Mycobacterium tuberculosis infection are associated with timing of
1306 reactivation. J Immunol *186*, 3527-3537.

1307 Mattila, J.T., Maiello, P., Sun, T., Via, L.E., and Flynn, J.L. (2015). Granzyme B-
1308 expressing neutrophils correlate with bacterial load in granulomas from Mycobacterium
1309 tuberculosis-infected cynomolgus macaques. Cell Microbiol *17*, 1085-1097.

1310 Mattila, J.T., Ojo, O.O., Kepka-Lenhart, D., Marino, S., Kim, J.H., Eum, S.Y., Via, L.E.,
1311 Barry, C.E., 3rd, Klein, E., Kirschner, D.E.*, et al.* (2013). Microenvironments in
1312 tuberculous granulomas are delineated by distinct populations of macrophage subsets
1313 and expression of nitric oxide synthase and arginase isoforms. J Immunol *191*, 773-784.

1314 McCaffrey, E.F., Donato, M., Keren, L., Chen, Z., Fitzpatrick, M., Jojic, V., Delmastro,
1315 A., Greenwald, N.F., Baranski, A., Graf, W.*, et al.* (2020). Multiplexed imaging of human
1316 tuberculosis granulomas uncovers immunoregulatory features conserved across tissue
1317 and blood. bioRxiv, 2020.2006.2008.140426.

1318 Meyer Zu Horste, G., Wu, C., Wang, C., Cong, L., Pawlak, M., Lee, Y., Elyaman, W.,
1319 Xiao, S., Regev, A., and Kuchroo, V.K. (2016). RBPJ Controls Development of
1320 Pathogenic Th17 Cells by Regulating IL-23 Receptor Expression. Cell Rep *16*, 392-404.

1321 Millington, K.A., Innes, J.A., Hackforth, S., Hinks, T.S., Deeks, J.J., Dosanjh, D.P.,
1322 Guyot-Revol, V., Gunatheesan, R., Klenerman, P., and Lalvani, A. (2007). Dynamic
1323 relationship between IFN-gamma and IL-2 profile of Mycobacterium tuberculosis-
1324 specific T cells and antigen load. J Immunol *178*, 5217-5226.

1325 Mogues, T., Goodrich, M.E., Ryan, L., LaCourse, R., and North, R.J. (2001). The
1326 relative importance of T cell subsets in immunity and immunopathology of airborne
1327 Mycobacterium tuberculosis infection in mice. J Exp Med *193*, 271-280.

1328 Montoro, D.T., Haber, A.L., Biton, M., Vinarsky, V., Lin, B., Birket, S.E., Yuan, F., Chen,
1329 S., Leung, H.M., Villoria, J.*, et al.* (2018). A revised airway epithelial hierarchy includes
1330 CFTR-expressing ionocytes. Nature *560*, 319-324.

1331 Mpande, C.A.M., Dintwe, O.B., Musvosvi, M., Mabwe, S., Bilek, N., Hatherill, M.,
1332 Nemes, E., Scriba, T.J., and Team, S.C.I. (2018). Functional, Antigen-Specific Stem

Cell Memory (TSCM) CD4(+) T Cells Are Induced by Human Mycobacterium tuberculosis Infection. Front Immunol *9*, 324.

Munoz-Elias, E.J., Timm, J., Botha, T., Chan, W.T., Gomez, J.E., and McKinney, J.D. (2005). Replication dynamics of Mycobacterium tuberculosis in chronically infected mice. Infect Immun *73*, 546-551.

Nathan, A., Beynor, J.I., Baglaenko, Y., Suliman, S., Ishigaki, K., Asgari, S., Huang, C.-C., Luo, Y., Zhang, Z., Tamara, K.L.*, et al.* (2020). Multimodal memory T cell profiling identifies a reduction in a polyfunctional Th17 state associated with tuberculosis progression. bioRxiv, 2020.2004.2023.057828.

Niedzielska, M., Israelsson, E., Angermann, B., Sidders, B.S., Clausen, M., Catley, M., Malhotra, R., and Dumont, C. (2018). Differential gene expression in human tissue resident regulatory T cells from lung, colon, and blood. Oncotarget *9*, 36166-36184.

O'Garra, A., Redford, P.S., McNab, F.W., Bloom, C.I., Wilkinson, R.J., and Berry, M.P. (2013). The immune response in tuberculosis. Annu Rev Immunol *31*, 475-527.

Ogongo, P., Steyn, A.J., Karim, F., Dullabh, K.J., Awala, I., Madansein, R., Leslie, A., and Behar, S.M. (2020). Differential skewing of donor-unrestricted and gammadelta T cell repertoires in tuberculosis-infected human lungs. J Clin Invest *130*, 214-230.

Ohtani, H. (2013). Granuloma cells in chronic inflammation express CD205 (DEC205) antigen and harbor proliferating T lymphocytes: similarity to antigen-presenting cells. Pathol Int *63*, 85-93.

Ordovas-Montanes, J., Dwyer, D.F., Nyquist, S.K., Buchheit, K.M., Vukovic, M., Deb, C., Wadsworth, M.H., 2nd, Hughes, T.K., Kazer, S.W., Yoshimoto, E.*, et al.* (2018). Allergic inflammatory memory in human respiratory epithelial progenitor cells. Nature *560*, 649-654.

Pagan, A.J., and Ramakrishnan, L. (2014). Immunity and Immunopathology in the Tuberculous Granuloma. Cold Spring Harb Perspect Med *5*.

Phuah, J., Wong, E.A., Gideon, H.P., Maiello, P., Coleman, M.T., Hendricks, M.R., Ruden, R., Cirrincione, L.R., Chan, J., Lin, P.L.*, et al.* (2016). Effects of B Cell Depletion on Early Mycobacterium tuberculosis Infection in Cynomolgus Macaques. Infect Immun *84*, 1301-1311.

Phuah, J.Y., Mattila, J.T., Lin, P.L., and Flynn, J.L. (2012). Activated B cells in the granulomas of nonhuman primates infected with Mycobacterium tuberculosis. Am J Pathol *181*, 508-514.

Portevin, D., Via, L.E., Eum, S., and Young, D. (2012). Natural killer cells are recruited during pulmonary tuberculosis and their ex vivo responses to mycobacteria vary between healthy human donors in association with KIR haplotype. Cell Microbiol *14*, 1734-1744.

1370 Prakadan, S.M., Shalek, A.K., and Weitz, D.A. (2017). Scaling by shrinking:
1371 empowering single-cell 'omics' with microfluidic devices. Nat Rev Genet *18*, 345-361.

1372 Raphael, I., Nalawade, S., Eagar, T.N., and Forsthuber, T.G. (2015). T cell subsets and
1373 their signature cytokines in autoimmune and inflammatory diseases. Cytokine *74*, 5-17.

1374 Reece, S.T., and Kaufmann, S.H. (2012). Floating between the poles of pathology and
1375 protection: can we pin down the granuloma in tuberculosis? Curr Opin Microbiol *15*, 63-
1376 70.

1377 Rodrigues, M., Kosaric, N., Bonham, C.A., and Gurtner, G.C. (2019). Wound Healing: A
1378 Cellular Perspective. Physiol Rev *99*, 665-706.

1379 Roy Chowdhury, R., Vallania, F., Yang, Q., Lopez Angel, C.J., Darboe, F., Penn-
1380 Nicholson, A., Rozot, V., Nemes, E., Malherbe, S.T., Ronacher, K.*, et al.* (2018). Author
1381 Correction: A multi-cohort study of the immune factors associated with M. tuberculosis
1382 infection outcomes. Nature *564*, E5.

1383 Rubinchik, E., and Levi-Schaffer, F. (1994). Mast cells and fibroblasts: two interacting
1384 cells. Int J Clin Lab Res *24*, 139-142.

1385 Russell, D.G., Barry, C.E., 3rd, and Flynn, J.L. (2010). Tuberculosis: what we don't
1386 know can, and does, hurt us. Science *328*, 852-856.

1387 Sakai, S., Kauffman, K.D., Sallin, M.A., Sharpe, A.H., Young, H.A., Ganusov, V.V., and
1388 Barber, D.L. (2016). CD4 T Cell-Derived IFN-gamma Plays a Minimal Role in Control of
1389 Pulmonary Mycobacterium tuberculosis Infection and Must Be Actively Repressed by
1390 PD-1 to Prevent Lethal Disease. PLoS Pathog *12*, e1005667.

1391 Schietinger, A., Delrow, J.J., Basom, R.S., Blattman, J.N., and Greenberg, P.D. (2012).
1392 Rescued tolerant CD8 T cells are preprogrammed to reestablish the tolerant state.
1393 Science *335*, 723-727.

1394 Scriba, T.J., Coussens, A.K., and Fletcher, H.A. (2017). Human Immunology of
1395 Tuberculosis. Microbiol Spectr *5*.

1396 Shehadeh, L.A., Yu, K., Wang, L., Guevara, A., Singer, C., Vance, J., and
1397 Papapetropoulos, S. (2010). SRRM2, a potential blood biomarker revealing high
1398 alternative splicing in Parkinson's disease. PLoS One *5*, e9104.

1399 Shen, L., Frencher, J., Huang, D., Wang, W., Yang, E., Chen, C.Y., Zhang, Z., Wang,
1400 R., Qaqish, A., Larsen, M.H.*, et al.* (2019). Immunization of Vgamma2Vdelta2 T cells
1401 programs sustained effector memory responses that control tuberculosis in nonhuman
1402 primates. Proc Natl Acad Sci U S A *116*, 6371-6378.

1403 Siddiqui, I., Schaeuble, K., Chennupati, V., Fuertes Marraco, S.A., Calderon-Copete, S.,
1404 Pais Ferreira, D., Carmona, S.J., Scarpellino, L., Gfeller, D., Pradervand, S.*, et al.*
1405 (2019). Intratumoral Tcf1(+)PD-1(+)CD8(+) T Cells with Stem-like Properties Promote

Tumor Control in Response to Vaccination and Checkpoint Blockade Immunotherapy. Immunity *50*, 195-211 e110.

Smillie, C.S., Biton, M., Ordovas-Montanes, J., Sullivan, K.M., Burgin, G., Graham, D.B., Herbst, R.H., Rogel, N., Slyper, M., Waldman, J.*, et al.* (2019). Intra- and Inter-cellular Rewiring of the Human Colon during Ulcerative Colitis. Cell *178*, 714-730 e722.

Szabo, P.A., Levitin, H.M., Miron, M., Snyder, M.E., Senda, T., Yuan, J., Cheng, Y.L., Bush, E.C., Dogra, P., Thapa, P.*, et al.* (2019). Single-cell transcriptomics of human T cells reveals tissue and activation signatures in health and disease. Nat Commun *10*, 4706.

Tabula Muris, C., Overall, c., Logistical, c., Organ, c., processing, Library, p., sequencing, Computational data, a., Cell type, a., Writing, g.*, et al.* (2018). Single-cell transcriptomics of 20 mouse organs creates a Tabula Muris. Nature *562*, 367-372.

Takeuchi, M., Ohno, K., Takata, K., Gion, Y., Tachibana, T., Orita, Y., Yoshino, T., and Sato, Y. (2015). Interleukin 13-positive mast cells are increased in immunoglobulin G4-related sialadenitis. Sci Rep *5*, 7696.

Taweevisit, M., and Poumsuk, U. (2007). High mast cell density associated with granulomatous formation in tuberculous lymphadenitis. Southeast Asian J Trop Med Public Health *38*, 115-119.

Tirosh, I., Izar, B., Prakadan, S.M., Wadsworth, M.H., 2nd, Treacy, D., Trombetta, J.J., Rotem, A., Rodman, C., Lian, C., Murphy, G.*, et al.* (2016). Dissecting the multicellular ecosystem of metastatic melanoma by single-cell RNA-seq. Science *352*, 189-196.

Tu, A.A., Gierahn, T.M., Monian, B., Morgan, D.M., Mehta, N.K., Ruiter, B., Shreffler, W.G., Shalek, A.K., and Love, J.C. (2019). TCR sequencing paired with massively parallel 3' RNA-seq reveals clonotypic T cell signatures. Nat Immunol *20*, 1692-1699.

Ulrichs, T., and Kaufmann, S.H. (2006). New insights into the function of granulomas in human tuberculosis. J Pathol *208*, 261-269.

van Hamburg, J.P., and Tas, S.W. (2018). Molecular mechanisms underpinning T helper 17 cell heterogeneity and functions in rheumatoid arthritis. J Autoimmun *87*, 69-81.

Van Rhijn, I., Godfrey, D.I., Rossjohn, J., and Moody, D.B. (2015). Lipid and small-molecule display by CD1 and MR1. Nat Rev Immunol *15*, 643-654.

Verreck, F.A., Vervenne, R.A., Kondova, I., van Kralingen, K.W., Remarque, E.J., Braskamp, G., van der Werff, N.M., Kersbergen, A., Ottenhoff, T.H., Heidt, P.J.*, et al.* (2009). MVA.85A boosting of BCG and an attenuated, phoP deficient M. tuberculosis vaccine both show protective efficacy against tuberculosis in rhesus macaques. PLoS One *4*, e5264.

1442 Wacleche, V.S., Goulet, J.P., Gosselin, A., Monteiro, P., Soudeyns, H., Fromentin, R.,
1443 Jenabian, M.A., Vartanian, S., Deeks, S.G., Chomont, N.*, et al.* (2016). New insights
1444 into the heterogeneity of Th17 subsets contributing to HIV-1 persistence during
1445 antiretroviral therapy. Retrovirology *13*, 59.

1446 Whibley, N., Tucci, A., and Powrie, F. (2019). Regulatory T cell adaptation in the
1447 intestine and skin. Nat Immunol *20*, 386-396.

1448 White, A.G., Maiello, P., Coleman, M.T., Tomko, J.A., Frye, L.J., Scanga, C.A., Lin,
1449 P.L., and Flynn, J.L. (2017). Analysis of 18FDG PET/CT Imaging as a Tool for Studying
1450 Mycobacterium tuberculosis Infection and Treatment in Non-human Primates. J Vis
1451 Exp.

1452 WHO (2019). Global Tuberculosis Report.

1453 Wijesundara, D.K., Tscharke, D.C., Jackson, R.J., and Ranasinghe, C. (2013). Reduced
1454 interleukin-4 receptor alpha expression on CD8+ T cells correlates with higher quality
1455 anti-viral immunity. PLoS One *8*, e55788.

1456 Wong, E.A., Evans, S., Kraus, C.R., Engelman, K.D., Maiello, P., Flores, W.J., Cadena,
1457 A.M., Klein, E., Thomas, K., White, A.G.*, et al.* (2020). IL-10 Impairs Local Immune
1458 Response in Lung Granulomas and Lymph Nodes during Early Mycobacterium
1459 tuberculosis Infection. J Immunol *204*, 644-659.

1460 Wong, E.A., Joslyn, L., Grant, N.L., Klein, E., Lin, P.L., Kirschner, D.E., and Flynn, J.L.
1461 (2018). Low Levels of T Cell Exhaustion in Tuberculous Lung Granulomas. Infect
1462 Immun *86*.

1463 Wu, C., Pot, C., Apetoh, L., Thalhamer, T., Zhu, B., Murugaiyan, G., Xiao, S., Lee, Y.,
1464 Rangachari, M., Yosef, N.*, et al.* (2013). Metallothioneins negatively regulate IL-27-
1465 induced type 1 regulatory T-cell differentiation. Proc Natl Acad Sci U S A *110*, 7802-
1466 7807.

1467 Wu, K., Li, Y., Zhang, S., Zhou, N., Liu, B., Pan, T., Zhang, X., Luo, H., Huang, Z., Li,
1468 X.*, et al.* (2019). Preferential Homing of Tumor-specific and Functional CD8+ Stem Cell-
1469 like Memory T Cells to the Bone Marrow. J Immunother *42*, 197-207.

1470 Wulff, B.C., and Wilgus, T.A. (2013). Mast cell activity in the healing wound: more than
1471 meets the eye? Exp Dermatol *22*, 507-510.

1472 Yang, X.O., Nurieva, R., Martinez, G.J., Kang, H.S., Chung, Y., Pappu, B.P., Shah, B.,
1473 Chang, S.H., Schluns, K.S., Watowich, S.S.*, et al.* (2008). Molecular antagonism and
1474 plasticity of regulatory and inflammatory T cell programs. Immunity *29*, 44-56.

1475 Yosef, N., Shalek, A.K., Gaublomme, J.T., Jin, H., Lee, Y., Awasthi, A., Wu, C.,
1476 Karwacz, K., Xiao, S., Jorgolli, M.*, et al.* (2013). Dynamic regulatory network controlling
1477 TH17 cell differentiation. Nature *496*, 461-468.

1478 Zemmour, D., Zilionis, R., Kiner, E., Klein, A.M., Mathis, D., and Benoist, C. (2018).
1479 Single-cell gene expression reveals a landscape of regulatory T cell phenotypes shaped
1480 by the TCR. Nat Immunol *19*, 291-301.

1481 Zhan, L., Tang, J., Sun, M., and Qin, C. (2017). Animal Models for Tuberculosis in
1482 Translational and Precision Medicine. Front Microbiol *8*, 717.

1483 Zilionis, R., Engblom, C., Pfirschke, C., Savova, V., Zemmour, D., Saatcioglu, H.D.,
1484 Krishnan, I., Maroni, G., Meyerovitz, C.V., Kerwin, C.M.*, et al.* (2019). Single-Cell
1485 Transcriptomics of Human and Mouse Lung Cancers Reveals Conserved Myeloid
1486 Populations across Individuals and Species. Immunity *50*, 1317-1334 e1310.
1487

Figure 1

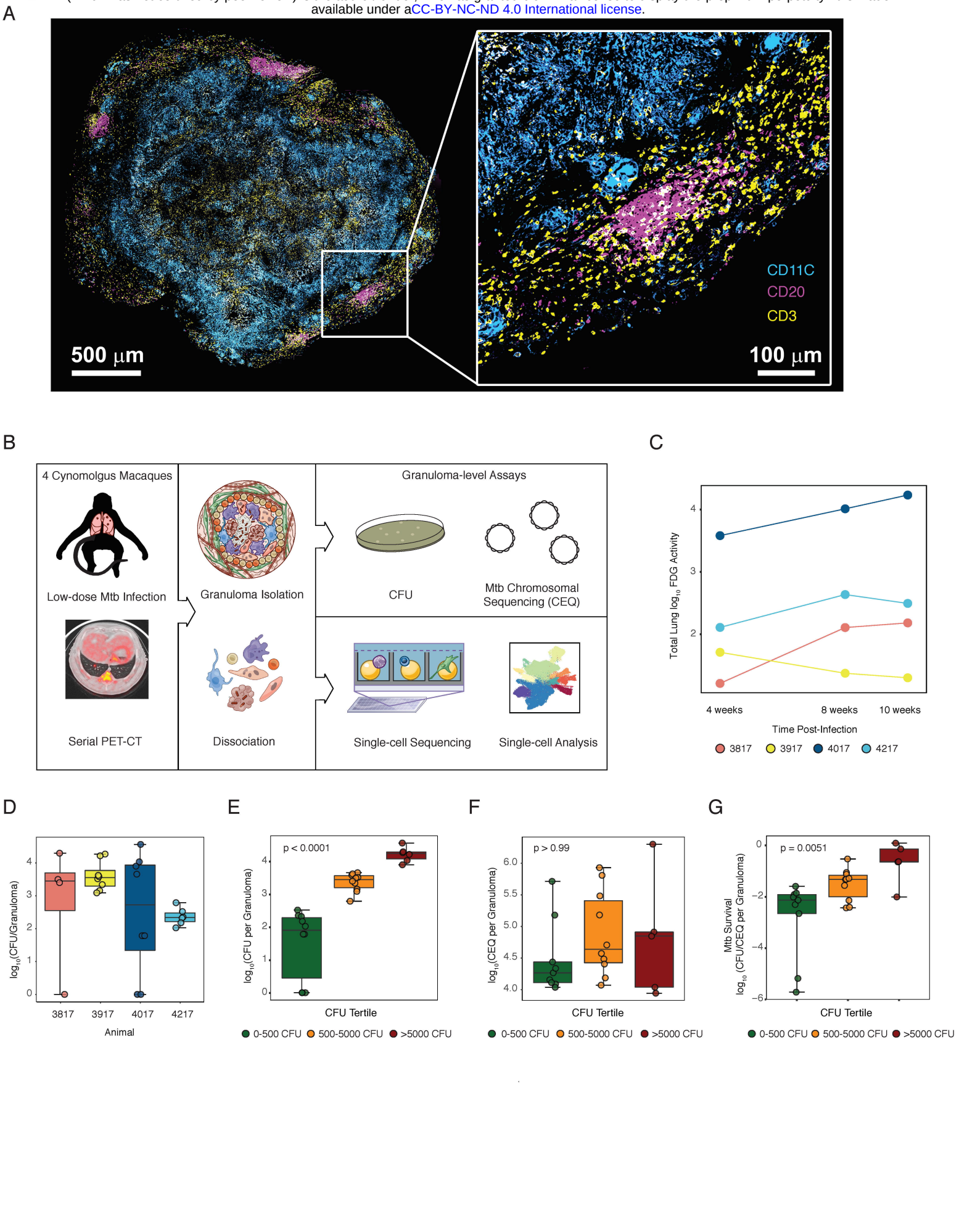

Figure 2

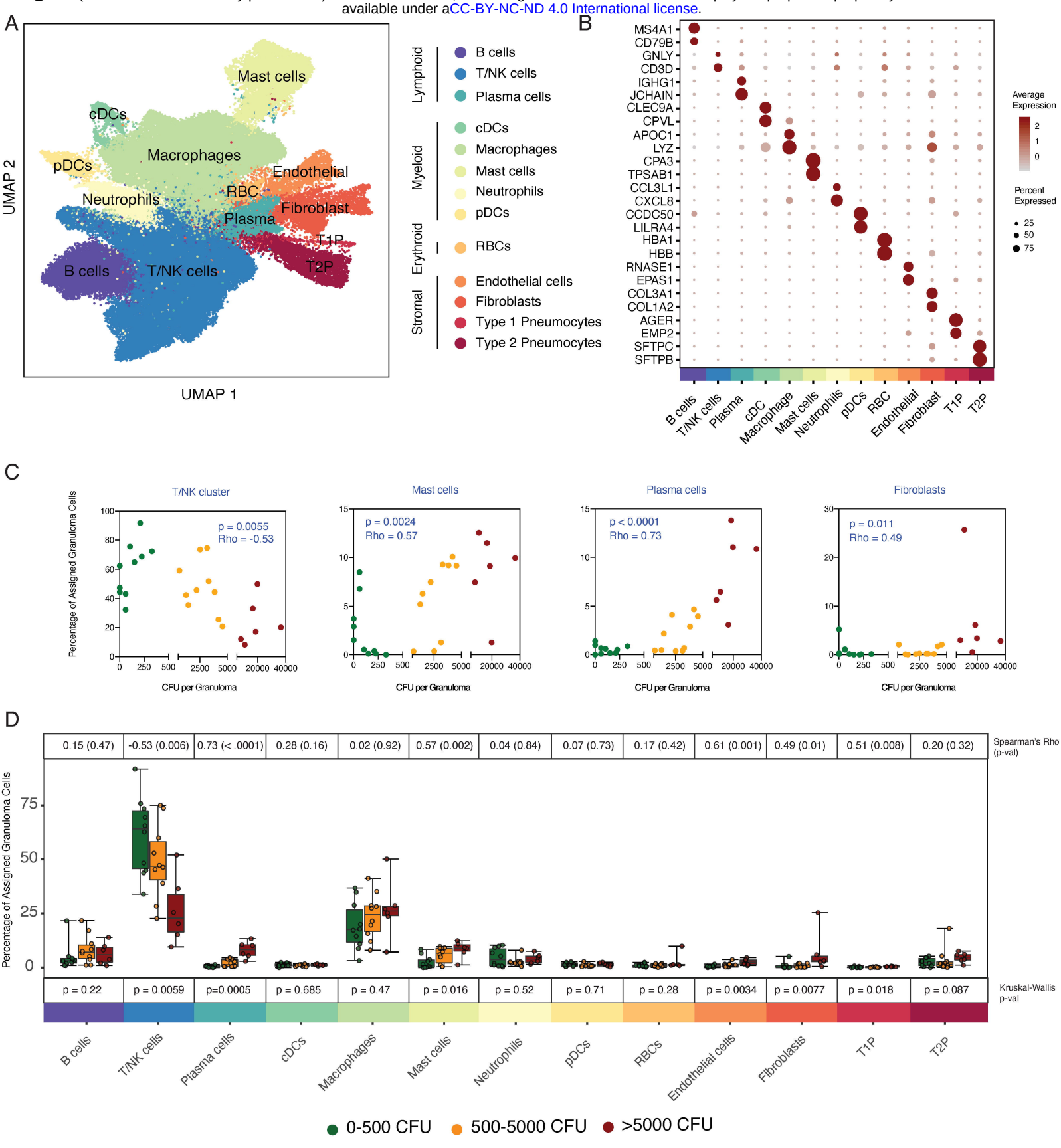

Figure 3.

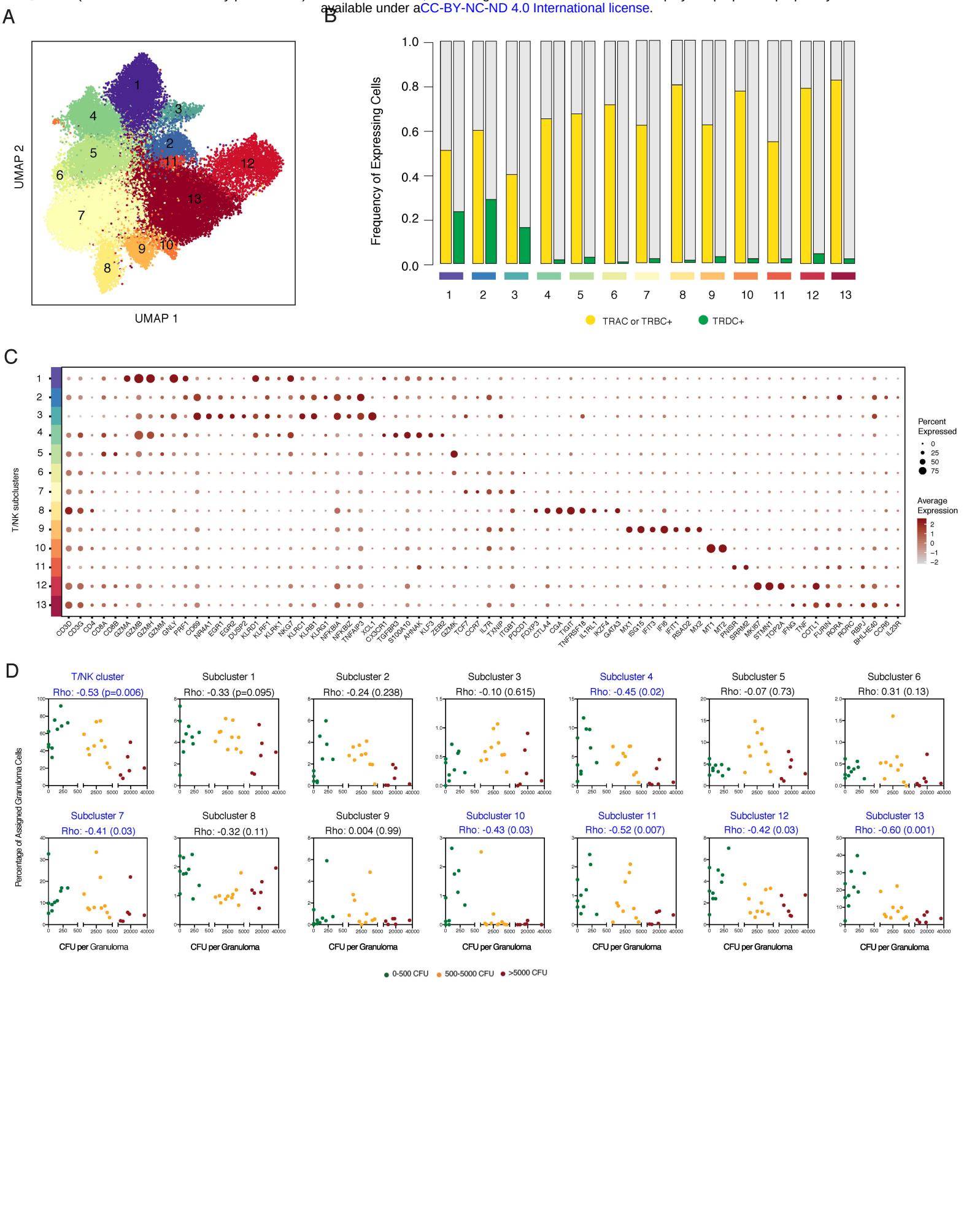

Figure 4.

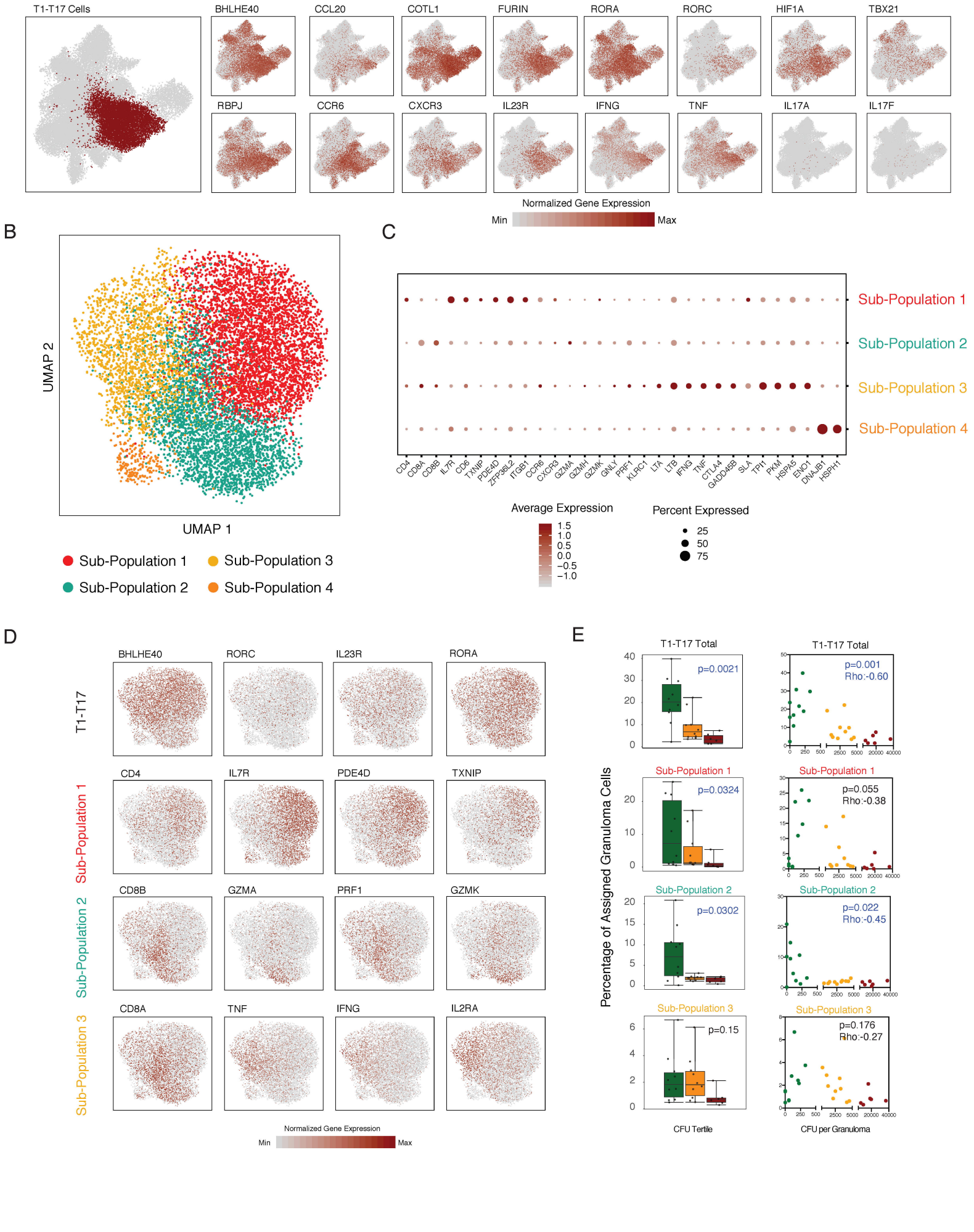

Figure 5.

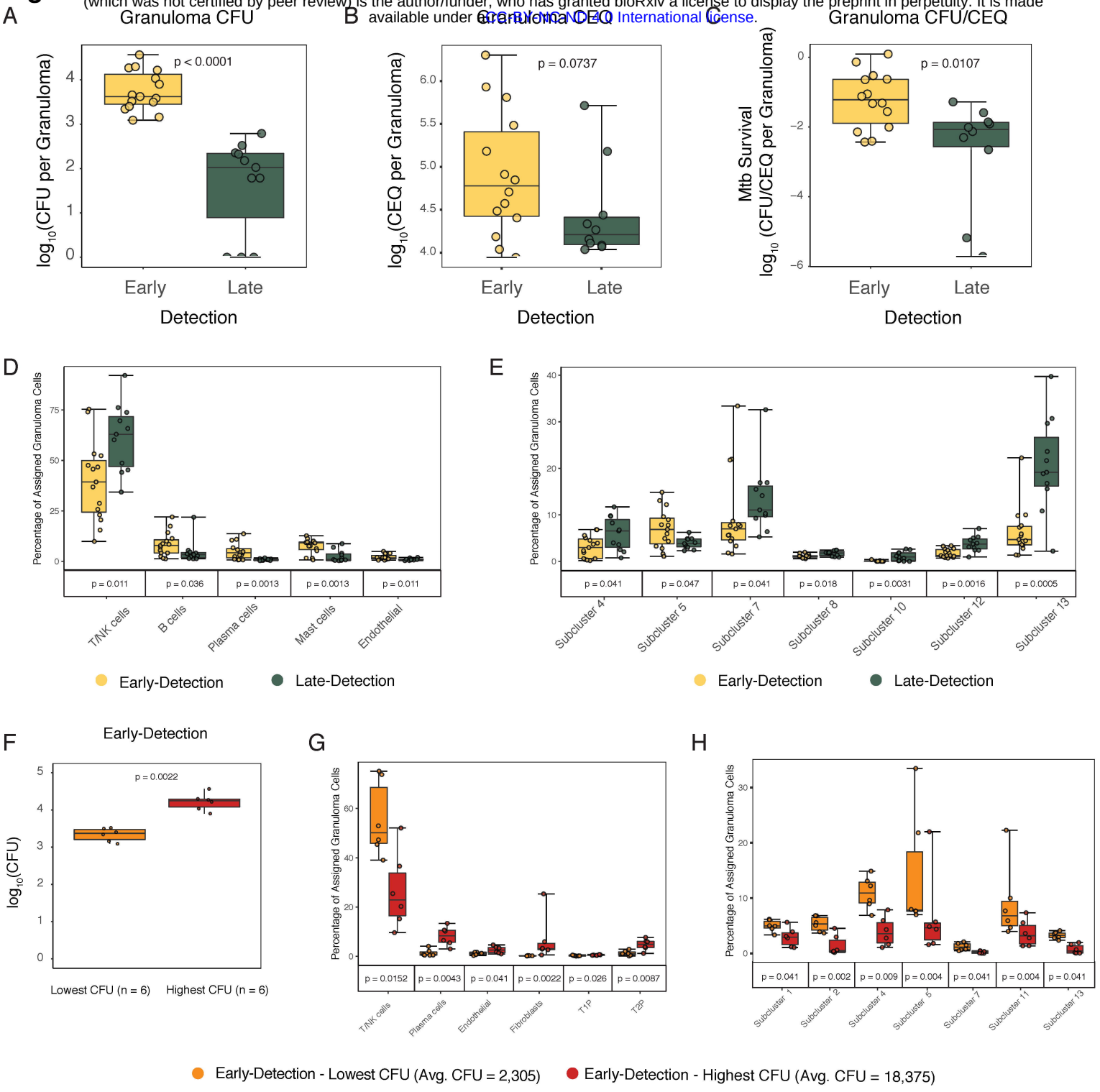

Figure 6: